

University of Alabama in Huntsville

LOUIS

Honors Capstone Projects and Theses

Honors College

4-7-2023

Experimental Investigation of a Unique Upper Pressure Side Film Cooling Arrangement Supplied by Two Separate Plenums for a Transonic Squealer Turbine Blade Tip

Grayson M. Fulmer

Follow this and additional works at: <https://louis.uah.edu/honors-capstones>

Recommended Citation

Fulmer, Grayson M., "Experimental Investigation of a Unique Upper Pressure Side Film Cooling Arrangement Supplied by Two Separate Plenums for a Transonic Squealer Turbine Blade Tip" (2023). *Honors Capstone Projects and Theses*. 800.
<https://louis.uah.edu/honors-capstones/800>

This Thesis is brought to you for free and open access by the Honors College at LOUIS. It has been accepted for inclusion in Honors Capstone Projects and Theses by an authorized administrator of LOUIS.

Experimental Investigation of a Unique Upper Pressure Side Film Cooling Arrangement Supplied by Two Separate Plenums for a Transonic Squealer Turbine Blade Tip

by

Grayson M. Fulmer

**An Honors Capstone
submitted in partial fulfillment of the requirements
for the Honors Diploma to**


The Honors College


of


The University of Alabama in Huntsville

04/07/2023

**Honors Capstone Director: Dr. Phillip M. Ligrani
Eminent Scholar in Propulsion, Professor of Mechanical and Aerospace Engineering**

	04/07/2023
Student	Date

	04/07/2023
Director	Date

	04/07/2023
Department Chair	Date

Honors College Dean	Date
---------------------	------



Honors College Frank Franz Hall
+1 (256) 824-6450 (voice)
+1 (256) 824-7339 (fax) honors@uah.edu

Honors Thesis Copyright Permission

This form must be signed by the student and submitted with the final manuscript. In presenting this thesis in partial fulfillment of the requirements for Honors Diploma or Certificate from The University of Alabama in Huntsville, I agree that the Library of this University shall make it freely available for inspection. I further agree that permission for extensive copying for scholarly purposes may be granted by my advisor or, in his/her absence, by the Chair of the Department, Director of the Program, or the Dean of the Honors College. It is also understood that due recognition shall be given to me and to The University of Alabama in Huntsville in any scholarly use which may be made of any material in this thesis.

Grayson Fulmer

Student Name (printed)



Student Signature

04/07/2023

Date

Table of Contents

Abstract	4
Nomenclature	5
Chapter 1: Background and Configuration	6
Chapter 2: Blade Mach Number Distributions	8
Chapter 3: Baseline Surface Heat Transfer Coefficient Distributions	9
Chapter 4: Line-Averaged Data Analysis Procedures for the Blade Surfaces	11
Chapter 5: Results with Film Cooling	13
5.1 Spatially-Resolved Film Cooling Effectiveness Distributions along the Squealer Tip Surface and Upper Pressure Side Surface	13
5.2 Spatially-Resolved Heat Transfer Coefficient Ratio Distributions along the Squealer Tip Surface and Upper Pressure Side Surface	14
5.3 Line-Averaged Adiabatic Film Cooling Effectiveness Distributions Along the Squealer Blade Tip Surface	16
5.4 Line-Averaged Adiabatic Film Cooling Effectiveness Distributions Along The Upper Pressure Side Blade Surface	19
5.5 Line-Averaged Heat Transfer Coefficient Ratio Distributions Along The Squealer Blade Tip Surface	20
5.6 Line-Averaged Heat Transfer Coefficient Ratio Distributions Along The Upper Pressure Side Blade Surface	21
5.7 Local Adiabatic Film Cooling Effectiveness Variations with Film Cooling Blowing Ratio Along Squealer Blade Tip Surface	22

5.8 Local Heat Transfer Coefficient Ratio Variations with Film Cooling Blowing	23
Ratio Along Squealer Blade Tip Surface	
Chapter 6: Summary and Conclusions	25
Figures	28
References	55

Abstract

Investigated is a new film cooling hole arrangement for the upper pressure side of the turbine blade to give improved thermal protection along blade tip regions (relative to previous configuration which have been investigated), as lower mass flow rates of the film coolant are employed (relative to previous configuration which have been investigated). Data include spatially-resolved and line-averaged distributions of heat transfer coefficient ratio and adiabatic film cooling effectiveness. Spatially-resolved surface heat transfer characteristics are measured using transient infrared thermography, and an impulse response transient measurement technique. Film coolant is supplied with a carbon dioxide injection system, as utilized within the 8D blade configuration film cooling holes. This arrangement is unique, relative to other film cooling configurations, because the of the following characteristics: (a) compound angle relative to the circumferential/axial plane, (b) inclination angle relative to a plane which is tangent to the local blade surface at the hole exit location, (c) two interior plenums used to independently supply film cooling to a group of upstream holes and to a group of downstream holes, (d) locations relative to the top of the pressure side squealer rim corner, and (e) number of holes along the upper pressure side of the blade with the same coolant supply arrangements. Results indicate that the heat transfer coefficient and adiabatic film cooling effectiveness distributions vary in a complex manner as the downstream blowing ratio is altered and the upstream blowing ratio is maintained approximately constant. In general, all three of the blowing ratio cases provide notable film coolant coverage within upstream portions of squealer recess regions, along portions of the pressure side rim region, and along the trailing edge region. The most pronounced variations of surface thermal characteristics with changes to the downstream blowing ratio are present for downstream portions of the blade, especially along the trailing edge region.

Nomenclature

BR	=	film cooling blowing ratio
BR_u	=	upstream plenum film cooling blowing ratio
BR_d	=	downstream plenum film cooling blowing ratio
C_x	=	axial chord length
h	=	iso-energetic heat transfer coefficient
h_o	=	baseline heat transfer coefficient
M	=	Mach number
P_s	=	static pressure
P_o	=	stagnation pressure
S	=	coordinate along the line represented by polynomial equation
S_o	=	coordinate along the line represented by polynomial equation from blade leading edge to trailing edge
x	=	upper pressure side axial/pitch coordinate
x'	=	upper pressure side axial/pitch coordinate
x_o	=	upper pressure side axial/pitch coordinate for normalization
y	=	upper pressure side radial coordinate
y'	=	upper pressure side radial coordinate
y_o	=	upper pressure side radial coordinate for normalization
η_{AD}	=	adiabatic film cooling effectiveness

Chapter 1: Background and Configuration

Investigated are the surface heat transfer characteristics of a film cooled transonic turbine squealer blade tip. A first-of-its-kind double plenum blade tip arrangement is investigated, which is denoted 8D. The present configuration is unique because the forward film cooling holes are supplied by an upstream plenum while the aft film cooling holes are supplied by a second downstream plenum. Data are provided which include spatially-resolved and line-averaged distributions of heat transfer coefficient ratio and adiabatic film cooling effectiveness. The effects of varying downstream blowing with a constant upstream blowing ratio on the surface heat transfer characteristics are investigated using an experimental apparatus and procedures highly similar to Collopy et al. (2022). The SS/TS/WT (supersonic/transonic/wind tunnel) blow down facility is employed with a transonic test section containing a five blade linear cascade. Spatially-resolved surface heat transfer characteristics are measured using transient infrared thermography, and an impulse response transient measurement technique. Film coolant is supplied with a carbon dioxide air gas mix injection system. Results indicate that heat transfer coefficient and adiabatic film cooling effectiveness distributions exhibit complex variation with alterations to the downstream blowing ratio as a constant upstream blowing ratio is maintained. In general, distributions and magnitudes of local adiabatic film cooling effectiveness indicate that all three blowing ratio cases with constant upstream blowing ratio provide reasonably good film coverage along the squealer tip surface for the trailing edge, recess and pressure side rim regions.

Figure 1 shows the schematic of linear cascade with dimensions given in mm. Shown in this figure are the locations of the central turbine blade which is instrumented, the circumferential bleed slots, and the tailboard. Radial bleed slots are also included at the cascade section inlet. A zinc-selenide window is located above the instrumented turbine

blade. Probes are located at the inlet of the cascade which are employed for measurement of mainstream total and static pressure and static temperature. The linear cascade consists of four flow passages with five complete blades.

The axial locations of 8D film cooling holes are given in Table 1. Figure 2 shows a diagram of the 8D configuration. Figure 2a gives the three-dimensional pressure side view of blade. Figure 2b shows the top view of blade. Details of 8D blade cooling configuration showing upstream and downstream plenums are provided in Figure 3. Note that the upstream plenum supplies the leading edge dusting hole and pressure side holes numbered 1 through 8. The downstream plenum supplies pressure side holes numbered 9 through 15 and the trailing edge dusting hole. With respect to the 8D blade geometry, the squealer depth of the 8D blade varies from 4.39 mm at the leading edge to 3.13 mm at the trailing edge. The tip gap employed in the present study is 1.2 mm.

Chapter 2: Blade Mach Number Distributions

Figure 4 shows central blade isentropic Mach number distributions. Figures 4a, 4b, 4c, and 4d correspond with the pressure surface at 50 percent span, the suction surface at 50 percent span, the pressure surface at 90 percent span, and the suction surface at 90 percent span, respectively. Figure 5 shows central blade static pressure to total pressure distributions. Figures 5a, 5b, 5c, and 5d correspond with the pressure surface at 50 percent span, the suction surface at 50 percent span, the pressure surface at 90 percent span, and the suction surface at 90 percent span, respectively. Here, measured data are represented by symbols. For the suction surfaces of the blade, data in these figures show that acceleration to sonic conditions occurs, followed by a deceleration to subsonic flow immediately downstream. The maximum Mach numbers for the 50 percent and 90 percent span locations are approximately 1.00, and 1.08, respectively. For the pressure surfaces of the blade, Fig. 4 again shows the presence of significant acceleration as the flow advects downstream, however, for these surfaces of the blade, the associated flow is subsonic along the entire length of the blade. The sudden acceleration of the flow (as illustrated by the Mach number variations in Fig. 4) are also associated with a significant drop in local static pressure, as shown by the pressure ratio results which are presented in Figure 5. Note that the resulting local static pressure gradients have important influences on local film coolant distributions, as well as upon associated surface adiabatic effectiveness and heat transfer coefficient values.

Chapter 3: Baseline Surface Heat Transfer Coefficient Distributions

Presented in Figure 6 are surface distributions of spatially-resolved heat transfer coefficients for a baseline squealer blade with no film cooling with a tip gap of 1.2 mm. Figure 6a shows the baseline blade heat transfer coefficient distribution along the squealer tip surface. Figure 6b shows the heat transfer coefficient distribution along the upper pressure side of the blade. Along the pressure side rim edge on the blade tip, present are high heat transfer coefficients due to enhanced shear stress and turbulence as the mainstream flow encounters pressure side corner. Within the recess region, the upstream 40 percent of the blade surface shows augmented heat transfer coefficient values similar to results from Viridi et al. (2013), where higher heat transfer coefficient values are attributed to subsonic flow and the influences of mid cavity vortices. According to Wheeler et al. (2011), locally higher speeds reduce heat transfer, relative to low-speed regions, in part, because of a reduction of local turbulence intensities, as a consequence of local flow accelerations. Also present are locally augmented heat transfer coefficient values within the squealer recess region, for x/C_x from approximately 0.6 to 0.75, parallel to the pressure side rim. This region shows evidence of locally augmented transfer coefficient values because of flow reattachment after separation from the inner pressure side rim corner. Relatively low heat transfer coefficients are then present along the suction side rim from x/C_x of 0.5 to 0.8 due to the presence of transonic flow. The trailing edge portion of the cavity (x/C_x of approximately 0.75) includes augmented heat transfer coefficients because of turbulent mixing which is augmented by the local stream wise pressure gradients. In regard to upper pressure side data, the heat transfer coefficient periodicity, evident as x'/x_0 varies in Figure 6b, is believed to be a consequence of disturbances from film cooling hole open exits. With the zero blowing ratio, no film cooling arrangement, no carbon dioxide or air flow is moving into or out of the film cooling holes.

Thus, disturbances from the open film cooling hole exits alter spatially resolved surface heat transfer coefficients locally by relatively small amounts. Along the squealer tip surface and along the upper pressure side surface, augmented values are due to changes in turbulence production and augmented local transport, which give enhanced local heat transfer coefficients.

Chapter 4: Line-Averaged Data Analysis Procedures for the Blade Surfaces

Line-averaged data distributions are determined from spatially-resolved surface distributions of adiabatic film cooling effectiveness and heat transfer coefficient ratio. Figure 7a shows how the line-averaging is implemented for the squealer tip surface. Using MATLAB version R2019a software, the first step is to determine polynomial equations (over the entire extent of the blade from the leading edge to the trailing edge), which are positioned along the edge of the pressure side rim, along the edge of suction side rim, through the center of the squealer recess region, and along the center of the trailing edge region. As illustrated by Figure 7a, line-averaging is then implemented in directions which are normal to the lines represented by these polynomial equations, over areas associated either with the pressure side rim, the suction side rim, and the squealer recess region. The coordinate along the line represented by each polynomial equation is denoted S/S_0 , which varies from 0.0 to 1.0, which respectively corresponds to a location near to the blade tip leading edge and to a location near to the blade trailing edge.

Surface distribution contour plots for the upper pressure side surface of the blade are obtained with an angled infrared camera mount. Because of this arrangement, resulting data are distributed over a plane with perspective and with surface curvature. The resulting spatially-resolved adiabatic film cooling effectiveness data and heat transfer coefficient ratio data are unwrapped and presented in a planar distribution, with a normal perspective view, by transforming pixel values as they are initially viewed by the infrared camera. MATLAB version R2019a software is employed for these transformations in several steps. After local data for the upper pressure surface of the blade are transformed, and provided in an unwrapped and planar arrangement, Figure 7b shows how data are line-averaged along straight lines. Associated coordinates are denoted x'/x_0 and y'/y_0 , where x_0 and y_0 is the length

and height of the region of consideration, respectively. Resulting data are given as they vary along the x'/x_0 direction, with line-averaging in the y'/y_0 direction. Resulting data are also given as they vary along the y'/y_0 direction, with line-averaging in the x'/x_0 direction. Also shown in Figure 7b is the x_0 quantity, which is the total length in the x direction, This quantity ranges from zero at a location near to the furthest upstream film cooling hole to one at a location near to the furthest downstream film cooling hole. Also shown in Figure 7b is the y_0 quantity, which is the total length in the y direction, ranging from zero at the film cooling hole centerlines to one at the top of the pressure side rim edge of the blade.

Chapter 5: Results with Film Cooling

Presented in the present chapter are results for: 5.1 Spatially-Resolved Film Cooling Effectiveness Distributions along the Squealer Tip Surface and Upper Pressure Side Surface, 5.2 Spatially-Resolved Heat Transfer Coefficient Ratio Distributions along the Squealer Tip Surface and Upper Pressure Side Surface, 5.3 Line-Averaged Adiabatic Film Cooling Effectiveness Distributions Along the Squealer Blade Tip Surface, 5.4 Line-Averaged Adiabatic Film Cooling Effectiveness Distributions Along The Upper Pressure Side Blade Surface, 5.5 Line-Averaged Heat Transfer Coefficient Ratio Distributions Along The Squealer Blade Tip Surface, 5.6 Line-Averaged Heat Transfer Coefficient Ratio Distributions Along The Upper Pressure Side Blade Surface, 5.7 Local Adiabatic Film Cooling Effectiveness Variations with Film Cooling Blowing Ratio Along Squealer Blade Tip Surface, and 5.8 Local Heat Transfer Coefficient Ratio Variations with Film Cooling Blowing Ratio Along Squealer Blade Tip Surface.

5.1 Spatially-Resolved Film Cooling Effectiveness Distributions along the Squealer Tip Surface and Upper Pressure Side Surface

Figure 8a shows adiabatic film cooling effectiveness distributions along the squealer tip surface with 8D film cooling for a tip gap of 1.2 mm with blowing ratios, $BR_u=1.89$ and $BR_d=1.04$. Figure 8b shows adiabatic film cooling effectiveness distributions along the upper pressure side with 8D film cooling for a tip gap of 1.2 mm with blowing ratios, $BR_u=1.94$ and $BR_d=0.97$. Within both figures, values of adiabatic film cooling effectiveness are equal to one at film exit plane locations. The highest local values of adiabatic film cooling effectiveness are then present at and near to dusting and pressure side hole exit locations and immediately downstream of dusting and pressure side hole exit locations.

With respect to the data in Figure 8a, as coolant emerges from the leading edge dusting hole, it collects in substantial amounts immediately downstream. Even further downstream from the leading edge dusting hole, there is substantial coverage in the upstream recess region from x/C_x of 0.1 to 0.45. With downstream development, the coolant trajectory provides more narrow coverage and remains within the pressure side corner of the recess region. For the trailing edge surface of the blade tip, there is large coverage of coolant within the vicinity of the trailing edge dusting hole.

Higher values of adiabatic film cooling effectiveness evidence larger amounts of coolant near to and along blade surfaces. Resulting coolant trajectories are then generally tied to local static pressure gradients and variations on the upper side of the blade and along the squealer tip surface. For both the squealer tip and the upper pressure side surface, effectiveness distributions are a result of the advection, distribution, and concentration of film coolant after it emerges from the 8D pressure side film cooling holes, advects outwards, turns downstream, and advects in an angular direction to the upper right, until the corner between the upper pressure side and pressure side squealer rim is encountered. For these regions, coolant advects along trajectories downstream of each hole in very high concentration, as shown by the data within Figure 8b.

5.2 Spatially-Resolved Heat Transfer Coefficient Ratio Distributions along the Squealer Tip Surface and Upper Pressure Side Surface

Figure 9a shows surface heat transfer coefficient distributions along the squealer tip surface with 8D film cooling for a tip gap of 1.2 mm with blowing ratios, $BR_u=1.89$ and $BR_d=1.04$. Figure 9b shows surface heat transfer coefficient ratio distributions along the upper pressure side surface with 8D film cooling for a tip gap of 1.2 mm with blowing ratios,

$BR_u=1.94$ and $BR_d=0.97$. Figure 10a shows surface heat transfer coefficient ratio distributions along the squealer tip surface with 8D film cooling for a tip gap of 1.2 mm with blowing ratios, $BR_u=1.89$ and $BR_d=1.04$. Figure 10b shows surface heat transfer coefficient ratio distributions along the upper pressure side surface with 8D film cooling for a tip gap of 1.2 mm with blowing ratios, $BR_u=1.94$ and $BR_d=0.97$.

Within Figures 9a and 9b, the highest values of heat transfer coefficient are present at the pressure side film cooling hole and squealer tip dusting hole locations. Local values of heat transfer coefficient are also augmented within the trailing edge portion of the cavity, and along the suction side rim for x/C_x locations of 0.10 to 0.30. Heat transfer coefficient ratio data, presented in Figure 10a, shows that values are very near to one along much of the squealer tip surface. Ratio values close to one, or equal to one, indicate that heat transfer coefficient data generally have variations which are similar to the baseline blade with no film cooling. Heat transfer coefficient ratio data evidence locally decreased heat transfer coefficients within the upstream 20 percent to 45 percent of the recess cavity and along a substantial portion of the pressure side rim. These deviations are due to locally diminished mixing and shear, and locally decreased turbulent transport. Local increases in heat transfer coefficient and heat transfer coefficient ratio are present along the upstream outer portion of the suction side rim, within the leading edge cavity region and along the trailing edge. Locally augmented heat transfer coefficient values are also evident at dusting hole exit locations, and around dusting hole exit locations associated with the leading edge and trailing edge dusting holes. These are due to increased turbulent transport from the advective presence of the film coolant.

When blade upper pressure side data are considered in Figure 10b, large values of heat transfer coefficient ratio are present at hole exit locations, and around and near to pressure side hole exit locations for both upstream and downstream collections of film cooling holes.

Reduced values of heat transfer coefficient (relative to a baseline blade with no film cooling) are present along downstream locations which follow the path of local coolant trajectories. This trend is especially pronounced for upstream pressure side holes from x'/x_0 of about 0.1 to 0.6.

5.3 Line-Averaged Adiabatic Film Cooling Effectiveness Distributions Along the Squealer Blade Tip Surface

Figures 11-14 show line-averaged adiabatic film cooling effectiveness variations with 8D film cooling, with blowing ratios cases $BR_u=1.89$ and $BR_d=1.04$, $BR_u=1.95$ and $BR_d=1.22$, and $BR_u=2.01$ and $BR_d=1.43$, with a tip gap of 1.2 mm. Figures 11, 12, 13, and 14 correspond with line-averaged data along the pressure side rim, along the squealer recess region, along the suction side rim, and along the trailing edge region, respectively.

Within Figure 11 along the pressure side rim region, there is notable coverage of coolant for all three downstream blowing ratios for S/S_0 from 0.15 to 0.9. There are distinct local peaks in line-averaged adiabatic film cooling effectiveness that are associated with each individual upstream pressure side film cooling hole. For S/S_0 locations between 0.5 and 0.9, the magnitudes of these peaks increase with increasing S/S_0 position due to additional accumulations of coolant as additional film cooling hole trajectories are encountered with streamwise development along the pressure side rim. With respect to variation in downstream blowing ratio as the upstream blowing ratio is maintained from 1.89 to 2.01, there is some deviation in values with changes in blowing ratio. As the downstream blowing ratio increases from 1.04 to 1.22, there is negligible change in line averaged adiabatic film cooling effectiveness. However, as the downstream blowing ratio is further increased to 1.43

there is an increase in line-averaged adiabatic film cooling effectiveness, especially for S/S_0 0.25 to 0.7, and again, between S/S_0 of 0.8 and 0.95 along the pressure side rim.

Within Figure 12, along the squealer recess region, there is substantial coverage of coolant associated with the leading edge dusting hole for most of the upstream recess region. Here, line-averaged adiabatic film cooling effectiveness peaks at the leading edge dusting hole location. Following this peak, there is a sharp decrease in line-averaged values followed by an increase to a second lower magnitude peak located near S/S_0 of 0.13. Beyond this location, line-averaged values generally decrease within the recess region as S/S_0 increases. Considering variations of downstream blowing ratio, as the upstream blowing ratio is maintained from 1.89 to 2.01, deviations in line-averaged values are apparent. As the downstream blowing ratio is increased from 1.04 to 1.22, line-averaged adiabatic film cooling effectiveness is only somewhat increased at the dusting hole exit location and at the second peak position. As the downstream blowing ratio is further increased to 1.43, decreases in line-averaged values for S/S_0 positions up to 0.15 are apparent. For S/S_0 position greater than 0.2, notable increases are present in line-averaged values for the blowing ratio of 1.43 relative to the other two cases.

Within Figure 13, along the suction side rim region, evidence of coverage of coolant for the upstream suction side rim is evident for S/S_0 positions between 0.1 and 0.4. For S/S_0 positions greater than 0.4, data indicate no coolant accumulations. As the downstream blowing ratio is increased from 1.04 to 1.22, the line-averaged adiabatic film cooling effectiveness values are largely unaffected. As the downstream blowing ratio is further increased to 1.43, substantial increases in line-averaged values around S/S_0 of 0.35 to 0.45 are present.

Within Figure 14, along the trailing edge region, large variations of line-averaged adiabatic film cooling effectiveness with increases in downstream blowing ratio are present. Data for downstream blowing ratios of 1.04, 1.22, and 1.43 evidence notable coolant coverage for S/S_0 locations beyond 0.2. Here, line-averaged values in general increase with increasing S/S_0 values up to 0.9. Line-averaged values peak at approximately 0.5 at an S/S_0 location of 0.9 which corresponds to the trailing edge dusting hole exit location. In general, line-averaged adiabatic film cooling effectiveness increases for most S/S_0 locations as the downstream blowing ratio becomes larger along the trailing edge region.

For the pressure side rim, squealer recess rim, suction side rim, and trailing edge region, complex variations of line-averaged adiabatic film cooling effectiveness with downstream blowing ratio are present. Although the upstream blowing ratio is nearly constant between 1.89 and 2.01, some variations in line-averaged adiabatic film cooling effectiveness are attributed to upstream plenum dusting holes and upstream pressure side holes. This is especially true for portions of the upstream recess, upstream pressure side rim, and upstream suction side rim regions. These changes are due to a small increase in the upstream blowing ratio of approximately 0.12. This increase in upstream blowing ratio is unavoidable due to the nature of the Harris regulator device used to control the supply pressure and set the upstream blowing ratio.

For the trailing edge portion, line-averaged adiabatic film cooling effectiveness values are affected by accumulations of coolant from both the upstream and downstream plenums. The most notable variations in line-averaged adiabatic film cooling effectiveness are due to varying downstream blowing ratio for most S/S_0 locations, as the upstream blowing ratio is held constant.

5.4 Line-Averaged Adiabatic Film Cooling Effectiveness Distributions Along The Upper Pressure Side Blade Surface

Figure 15 shows the variation of adiabatic film cooling effectiveness with y'/y_0 (with averaging in the x'/x_0 direction) with blowing ratio for a tip gap of 1.2 mm along the upper pressure side of the 8D blade. Figure 16 shows the variation of adiabatic film cooling effectiveness with x'/x_0 (with averaging in the y'/y_0 direction) with blowing ratio for a tip gap of 1.2 mm along the upper pressure side of the 8D blade. The data in Figures 15 and 16 are provided for blowing ratio cases of $BR_u=1.94$ and $BR_d=0.97$, $BR_u=1.83$ and $BR_d=1.18$, and $BR_u=1.93$ and $BR_d=1.43$.

Within Figure 15, variations of adiabatic film cooling effectiveness with x'/x_0 (with averaging in the y'/y_0 direction) for all blowing ratio cases exhibit periodic variations. The local maxima which occur are associated with individual pressure side hole exit locations. Note that the periodic variations associated with the upstream eight pressure side holes have large increases in values with sharp decreases in between hole exit locations to near zero values. However, when pressure side holes connected to the downstream plenum are considered, the local maxima associated with hole exit locations are less distinct with a much higher adiabatic effectiveness in between hole exit locations. There is little variation of adiabatic film cooling effectiveness with x'/x_0 (with averaging in the y'/y_0 direction) with changes to the downstream blowing ratio for the upstream eight pressure side holes. For the downstream plenum pressure side holes there is some variation in values with changes to downstream blowing ratio, especially for x'/x_0 locations greater than 0.8.

Within Figure 16, variations of adiabatic film cooling effectiveness with y'/y_0 (with averaging in the x'/x_0 direction) generally show a local maximum for y'/y_0 locations from 0.1 to 0.4. This is positioned near the downstream exits of the film cooling holes. As y'/y_0

increases further, line-averaged adiabatic effectiveness then generally decreases as the upper pressure side corner is approached. Complex variations adiabatic film cooling effectiveness with y'/y_0 (with averaging in the x'/x_0 direction) are present, with changes to downstream blowing ratio, as the upstream blowing ratio is maintained from 1.83 to 1.94. The data associated with the lowest downstream blowing ratio, $BR_d=0.97$, show the highest values overall for y'/y_0 up to around 0.4. For y'/y_0 locations from 0.4 to 0.9, the opposite trend is evident as the data associated with the highest downstream blowing ratio, BR_u of 1.43, show the highest values of line-averaged adiabatic film cooling effectiveness.

5.5 Line-Averaged Heat Transfer Coefficient Ratio Distributions Along The Squealer Blade Tip Surface

Figures 17-20 show line-averaged heat transfer coefficient ratio data for 8D film cooling, with blowing ratios cases $BR_u=1.89$ and $BR_d=1.04$, $BR_u=1.95$ and $BR_d=1.22$, and $BR_u=2.01$ and $BR_d=1.43$, for a tip gap of 1.2 mm. Figures 17, 18, 19, and 20 correspond with line-averaged data along the pressure side rim, along the squealer recess region, along the suction side rim, and along the trailing edge region, respectively.

The line-averaged heat transfer coefficient ratio data in Figures 17, 18, and 19 show some variations with location, depending upon the region of consideration. Generally, with several exceptions, ratio data are near to one, with some small local variations for different downstream blowing ratio values and for different S/S_0 values. Within Figure 17, along the pressure side rim region there is some variation in line averaged heat transfer coefficient ratio with changes to downstream blowing ratio as the upstream blowing ratio is maintained nearly constant from 1.89 to 2.01. The data associated with the highest downstream blowing ratio, $BR_u=2.01$, $BR_d=1.43$, exhibits slightly lower values for S/S_0 locations 0.3 to 0.8, relative to the

other two blowing ratio cases. Within Figure 18, there is a sharp spike in line-averaged ratio values at the leading edge dusting hole location, followed by a drop in ratio values. These deviations in line-averaged heat transfer coefficient ratio values are associated with film coolant trajectory paths and accumulations, and local variations of turbulent transport magnitudes.

5.6 Line-Averaged Heat Transfer Coefficient Ratio Distributions Along The Upper Pressure Side Blade Surface

Figure 21 shows the variation of heat transfer coefficient ratio with x'/x_0 (with averaging in the y'/y_0 direction) with blowing ratio for a tip gap of 1.2 mm along the upper pressure side of the 8D blade. Figure 22 shows the variation of heat transfer coefficient ratio with y'/y_0 (with averaging in the x'/x_0 direction) with blowing ratio for a tip gap of 1.2 mm along the upper pressure side of the 8D blade. Data in Figures 21 and 22 are provided for blowing ratio cases, $BR_u=1.94$ and $BR_d=0.97$, $BR_u=1.83$ and $BR_d=1.18$, and $BR_u=1.93$ and $BR_d=1.43$. Within Figure 21, more pronounced variations of heat transfer coefficient ratio with x'/x_0 (with averaging in the y'/y_0 direction) are present, with changes due to downstream blowing ratio for a nearly constant upstream blowing ratio. Here, changes are more pronounced in the vicinity of pressure side hole exit locations, where increases in heat transfer coefficient ratios with increasing blowing ratio are evident. In the locations between film cooling holes, for all blowing ratio cases, $BR_u=1.94$ and $BR_d=0.97$, $BR_u=1.83$ and $BR_d=1.18$, and $BR_u=1.93$ and $BR_d=1.43$, ratio values are in the vicinity of one.

Figure 22 shows complex variations of heat transfer coefficient ratio with blowing ratio in the vicinity of the exits of the film cooling holes. For y'/y_0 between 0 and 0.6, the heat transfer coefficient ratio associated with $BR_u=1.94$ and $BR_d=0.97$ decreases with increasing

y'/y_0 value. However, for blowing ratio cases, $BR_u=1.93$ and $BR_d=1.43$, as well as $BR_u=1.83$ and $BR_d=1.18$, heat transfer coefficient ratio values increase up to y'/y_0 of around 0.3. Following that, values for both blowing ratio cases then decrease with increasing y'/y_0 position up to y'/y_0 of around 0.9. For all three blowing ratio cases considered, ratio values are in the vicinity of one beyond y'/y_0 of 0.9 as the upper pressure side corner is approached.

5.7 Local Adiabatic Film Cooling Effectiveness Variations with Film Cooling Blowing Ratio Along Squealer Blade Tip Surface

The data within the present section are provided along surface lines which vary along the squealer blade tip. These lines are identified using the letters A, B, C, and D, where locations are shown in Figure 23. The adiabatic film cooling effectiveness data within Figure 23 are provided along the squealer blade tip with film cooling with $BR_u=1.89$ and $BR_d=1.04$. Figures 24a, 24b, 24c, and 24d then show the associated local, line-variations of adiabatic film cooling effectiveness, along the squealer tip surface, for blowing ratios cases $BR_u=1.89$ and $BR_d=1.04$, $BR_u=1.95$ and $BR_d=1.22$, $BR_u=2.01$ and $BR_d=1.43$ with a tip gap of 1.2 mm. Within these figures, vertical lines denote interior and exterior edges of both the pressure side rim and the suction side rim. The highest local values of film cooling effectiveness within these figures are present within the recess rim downstream of the leading edge dusting hole, and near the trailing edge region in the vicinity of the trailing edge dusting hole. Associated maximum values are as large as around 0.5. Data for line locations A and D in Figs. 24a and 24d show that local adiabatic film cooling effectiveness values generally increase along the trailing edge region as downstream blowing ratio increases (as the upstream blowing ratio is maintained nearly constant from 1.89 to 2.01).

Surface effectiveness characteristics and gradients provide evidence of the trajectories and distributions of the film, as it advects in a downstream direction after it emerges from the pressure side film coolant holes, encounters the blade corner, and then, turns, to subsequently advect along the pressure side squealer rim. A substantial amount of the film then advects from the pressure side to locations along the surface of the blade near the trailing edge. Film cooling distributions also emerge from the leading edge dusting hole and collect in high concentrations immediately downstream. With downstream development, this coolant provides large coverage in the upstream recess region up to x/C_x of around 0.45. Even further downstream, there continues to be narrow coverage along the pressure side of the recess cavity. Such coolant trajectory characteristics are illustrated and evidenced by adiabatic film cooling effectiveness data along lines A, B, C, and D, as these data are provided for varying blowing ratio conditions.

5.8 Local Heat Transfer Coefficient Ratio Variations with Film Cooling Blowing Ratio Along Squealer Blade Tip Surface

The data within the present section are provided along surface lines which vary along the squealer blade tip. These lines are identified using the letters A, B, C, and D, where locations are shown in Figure 25. The heat transfer coefficient ratio data within Figure 25 are provided along the squealer blade tip with film cooling with $BR_u=1.89$ and $BR_d=1.04$. Figures 26a, 26b, 26c, and 26d then show the associated local, line-variations of heat transfer coefficient ratios, along the squealer tip surface, for blowing ratios cases $BR_u=1.89$ and $BR_d=1.04$, $BR_u=1.95$ and $BR_d=1.22$, and $BR_u=2.01$ and $BR_d=1.43$ with a tip gap of 1.2 mm. Within these figures, vertical lines denote interior and exterior edges of both the pressure side rim and the suction side rim.

Data for line locations B and C in Figures 24b and 24c show that local heat transfer coefficient ratio values generally vary little as downstream blowing ratio increases (as the upstream blowing ratio is maintained nearly constant from 1.89 to 2.01). Data for line locations A and D for the trailing edge region in Figures 24a and 24d show more complex variations of local heat transfer coefficient ratio values as downstream blowing ratios are altered. For line location D in Figure 24d, for x/C_x up to 0.86, the lowest values are associated with the downstream blowing ratio $BR_d=1.22$, whereas the highest local ratio values are associated with downstream blowing ratio $BR_d=1.43$.

Chapter 6: Summary and Conclusions

The present study is aimed to achieve improved film cooling performance with increased surface areas with enhanced thermal protection for a transonic squealer turbine blade tip. A novel film cooling configuration, denoted 8D, with dusting holes along the squealer blade tip and pressure side holes, is considered. The 8D cooling scheme is unique because it employs two interior plenums to independently supply film cooling to a group of upstream holes and to a group of downstream holes. Within the present study, the upstream blowing ratio is maintained nearly constant with blowing ratios ranging from 1.83 to 2.01, as the downstream blowing ratio is altered from 0.97 to 1.43. Spatially-resolved surface heat transfer coefficients and surface adiabatic film cooling effectiveness distributions are presented for different downstream blowing ratio values. Results indicate that the heat transfer coefficient and adiabatic film cooling effectiveness distributions vary in a complex manner as the downstream blowing ratio is altered. In general, all three of the blowing ratio cases provide notable film coolant coverage within upstream portions of squealer recess regions, along portions of the pressure side rim region, and along the trailing edge region. The most pronounced variations of surface thermal characteristics with changes to the downstream blowing ratio are present for downstream portions of the blade, especially along the trailing edge region.

Spatially resolved, line-averaged, and local line-varying adiabatic film cooling effectiveness distributions for the 8D blade, show that, as the coolant emerges from the leading edge dusting hole, it collects in substantial amounts immediately downstream. Even further downstream from the leading edge dusting hole, substantial coolant coverage is present within the upstream portions of the recess region for x/C_x of 0.1 to 0.45. With additional downstream development, the coolant trajectory provides more narrow coverage

and remains present in the vicinity of the pressure side corner of the recess region. For the trailing edge surface of the blade tip, substantial coolant coverage and substantial effectiveness values are present within the vicinity of the trailing edge dusting hole. Here, significant variations of line-averaged and local line-varying adiabatic film cooling effectiveness values are present as the downstream blowing ratio is altered. Along this trailing edge region, the highest values of line-averaged adiabatic film cooling effectiveness are generally associated with the highest downstream blowing ratio BR_d of 1.43.

Along the upper pressure side surface of the blade, variations of adiabatic film cooling effectiveness with x'/x_0 (with averaging in the y'/y_0 direction) for all blowing ratio cases exhibit periodic variations. The local maxima which occur are associated with individual pressure side hole exit locations. Note that the periodic variations associated with the upstream eight pressure side holes have large increases in values with sharp decreases in between hole exit locations to near zero values. However, when pressure side holes connected to the downstream plenum are considered, the local maxima associated with hole exit locations are less distinct with a much higher adiabatic effectiveness in between hole exit locations. Here, there is little variation of adiabatic film cooling effectiveness with x'/x_0 (with averaging in the y'/y_0 direction) with changes to the downstream blowing ratio for the upstream eight pressure side holes. Variations of adiabatic film cooling effectiveness with y'/y_0 (with averaging in the x'/x_0 direction) generally show a local maximum for y'/y_0 locations from 0.1 to 0.4. This is positioned near the downstream exits of the film cooling holes. As y'/y_0 increases further, line-averaged adiabatic effectiveness then generally decreases as the upper pressure side corner is approached. Complex variations adiabatic film cooling effectiveness with y'/y_0 (with averaging in the x'/x_0 direction) are thus present, with

changes to downstream blowing ratio, as the upstream blowing ratio is maintained approximately constant from 1.83 to 1.94.

Line-averaged and local line-varying surface heat transfer coefficient ratios along the pressure side rim region, squealer recess region, suction side rim region, and trailing edge region show some deviations from baseline values for different locations as different blowing ratios are considered. In general, the deviations of heat transfer coefficients from baseline values (giving ratios different from 1.0), as the downstream blowing ratio is altered, are mostly due to local alterations to mixing and shear, and changes to local turbulent transport, which are related to the advective presence of the coolant. When the upper pressure side surface is considered, present are complex variations of heat transfer coefficient ratios with changes to downstream blowing ratio. For y'/y_0 between 0 and 0.6, heat transfer coefficient ratios associated with $BR_u=1.94$ and $BR_d=0.97$ decrease as spanwise position y'/y_0 becomes larger. For blowing ratio cases, $BR_u=1.93$ and $BR_d=1.43$, as well as $BR_u=1.83$ and $BR_d=1.18$, heat transfer coefficient ratio values increase as y'/y_0 increases to around 0.3. As y'/y_0 becomes larger to reach values in the vicinity of 0.9, values for both blowing ratio cases then decrease with increasing y'/y_0 spanwise position.

Figures

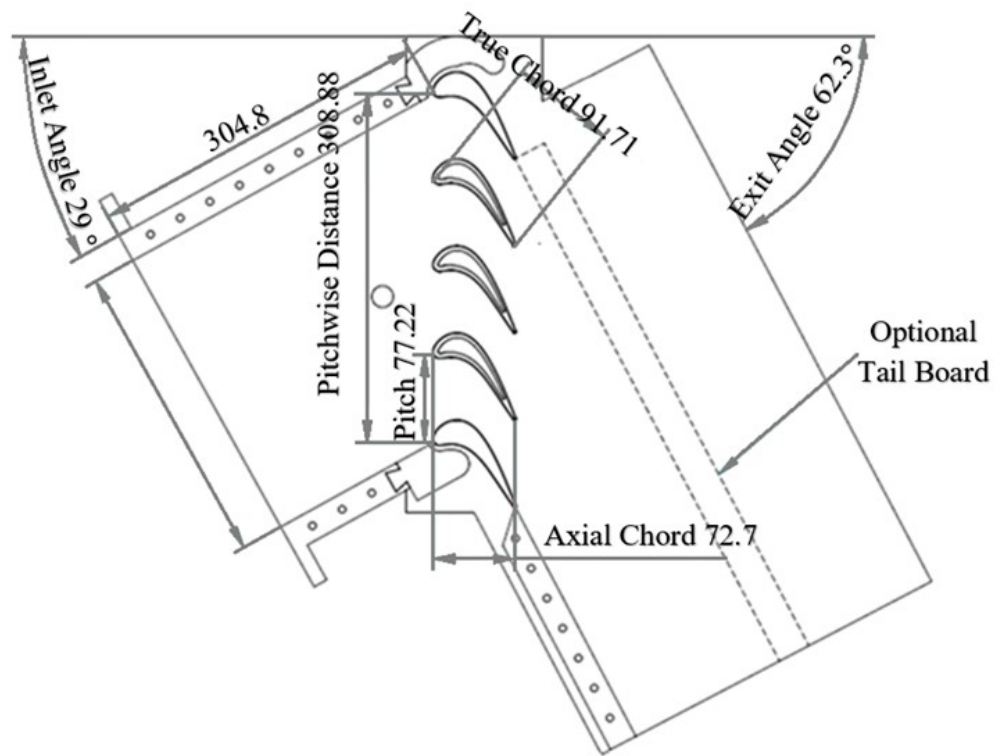


Figure 1. Schematic of linear cascade with dimensions given in mm.

Plenum	Film Cooling Hole Type	x/C_x
Upstream	LE Dusting Hole	0.098
Upstream	PS 1	0.388
Upstream	PS 2	0.469
Upstream	PS 3	0.541
Upstream	PS 4	0.583
Upstream	PS 5	0.623
Upstream	PS 6	0.663
Upstream	PS 7	0.704
Upstream	PS 8	0.745
Downstream	PS 9	0.783
Downstream	PS 10	0.804
Downstream	PS 11	0.825
Downstream	PS 12	0.846
Downstream	PS 13	0.868
Downstream	PS 14	0.897
Downstream	PS 15	0.945
Downstream	TE Dusting Hole	0.962

Table 1. Axial locations of 8D film cooling holes.

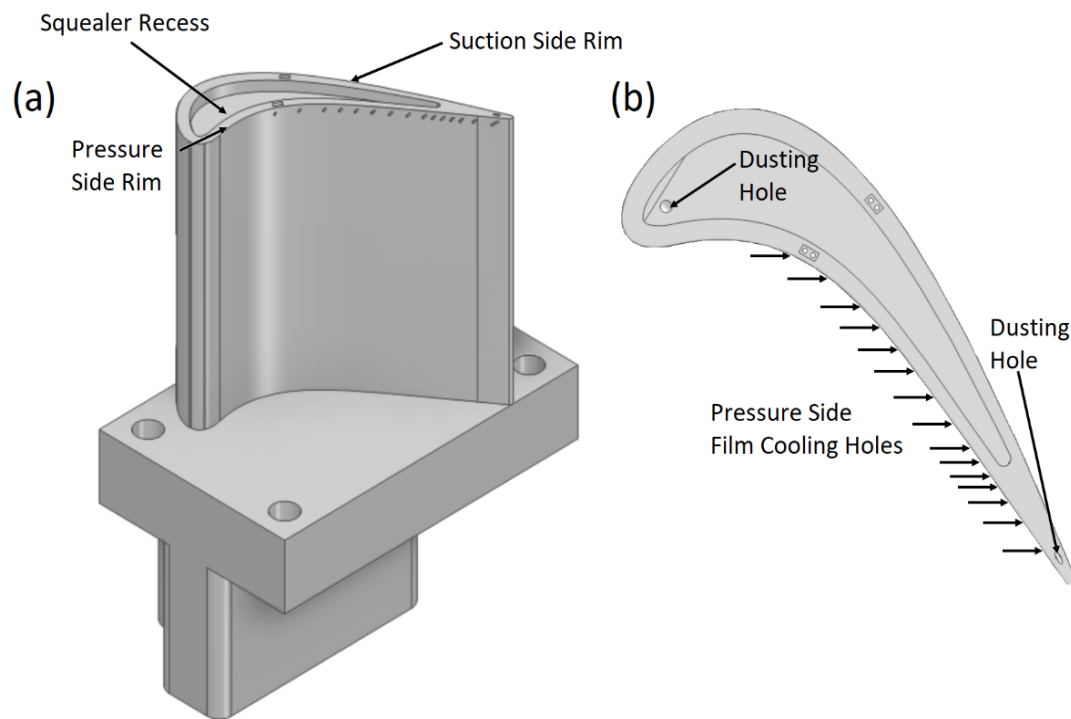


Figure 2. Diagram of blade. (a) Three-dimensional pressure side view of blade. (b) Top view of blade.

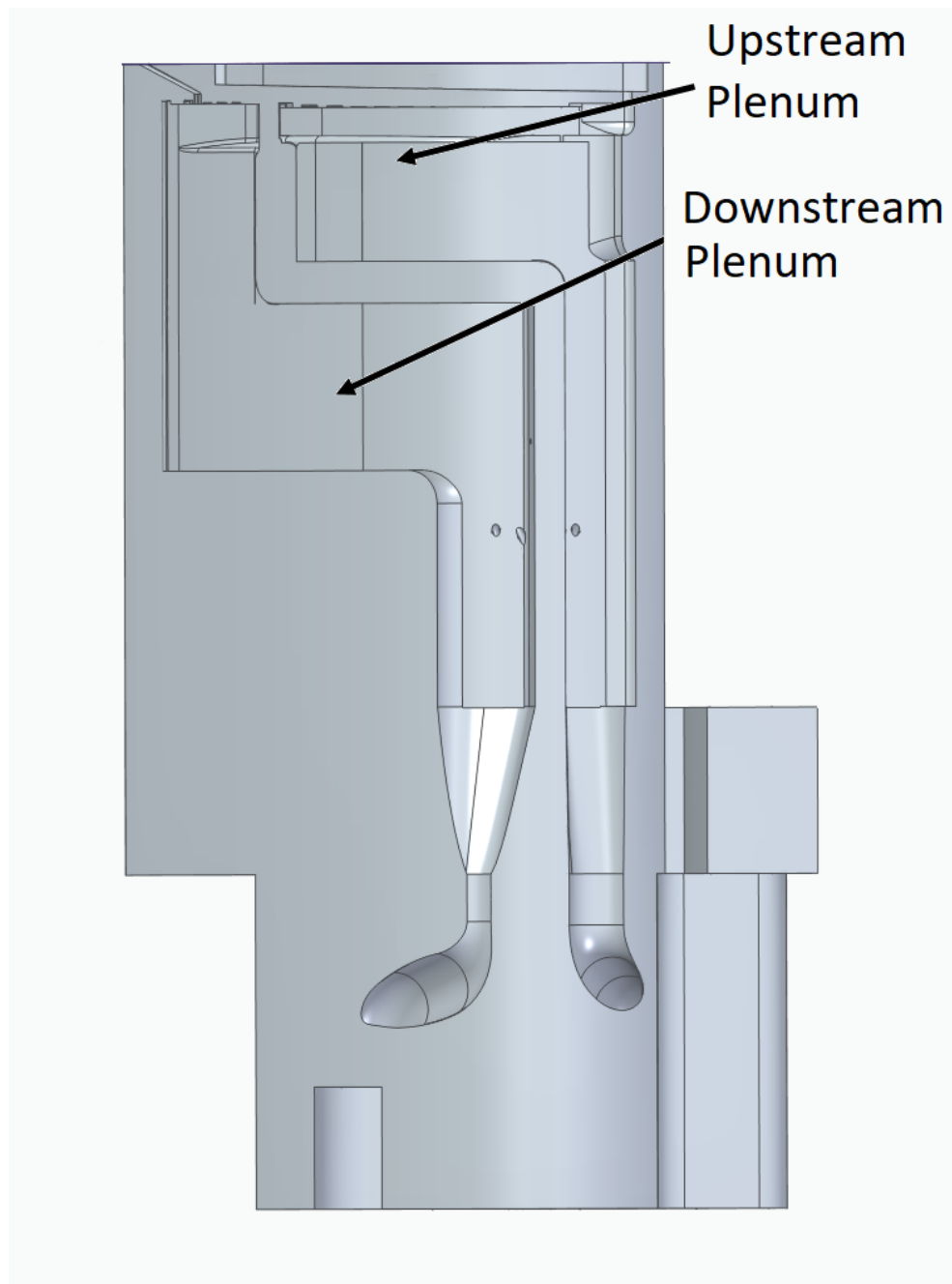


Figure 3. Details of 8D blade cooling configuration showing upstream and downstream plenums.

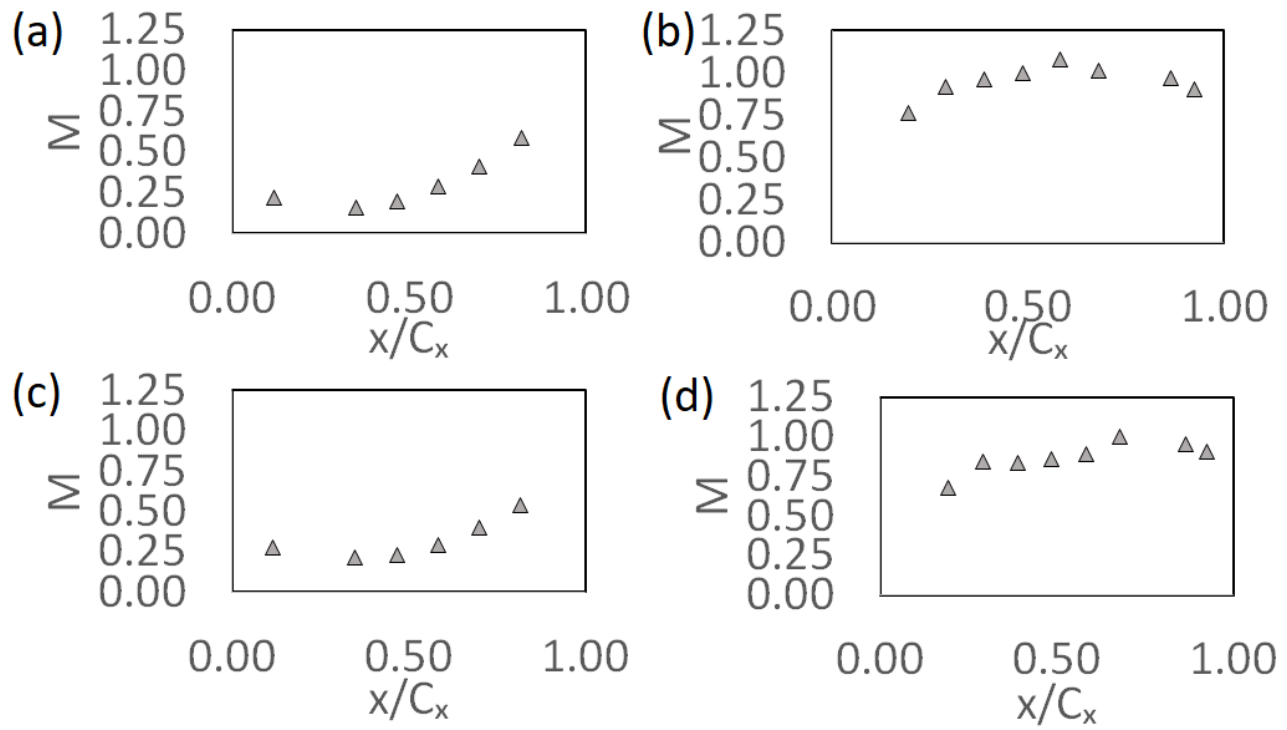


Figure 4. Central blade isentropic Mach number distributions with 1.2 mm tip gap for: (a) pressure surface at 50 percent span, (b) suction surface at 50 percent span, (c) pressure surface at 90 percent span, (d) suction surface at 90 percent span.

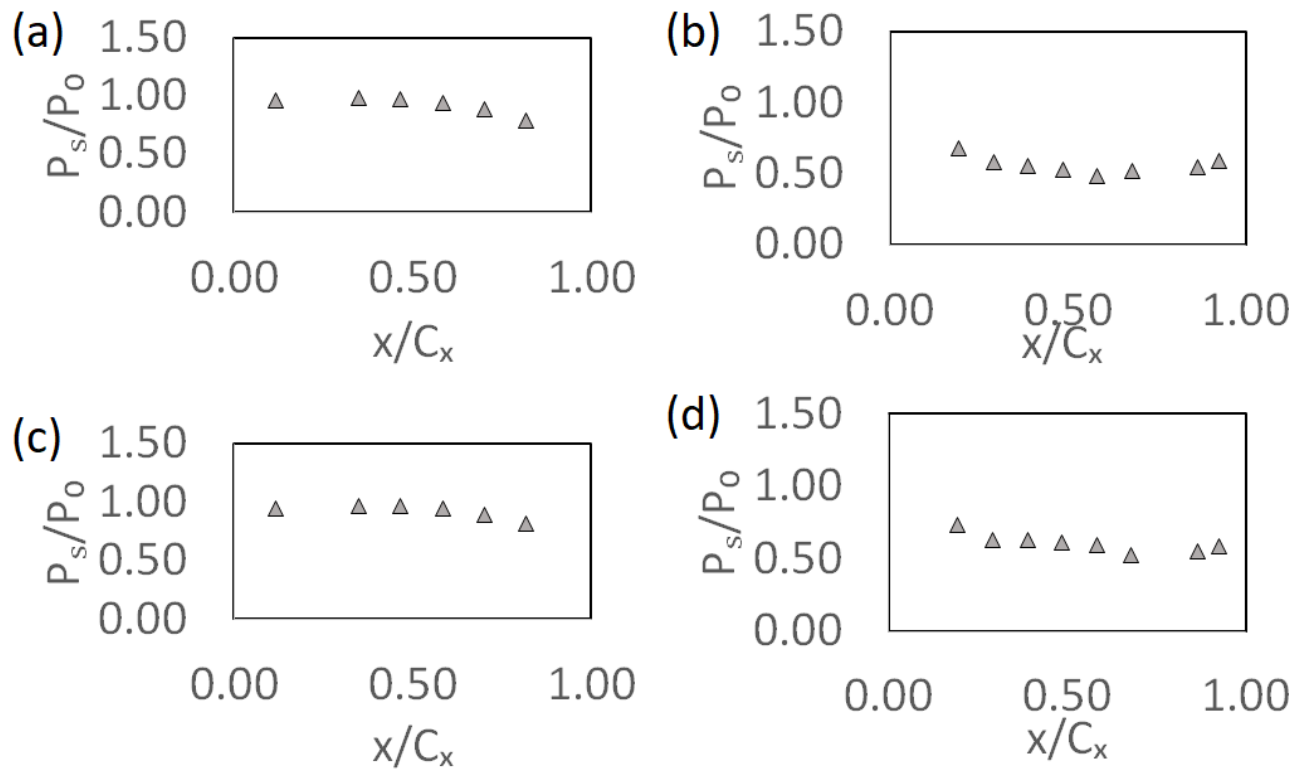


Figure 5. Central blade ratio of static pressure to stagnation pressure distributions with 1.2 mm tip gap for: (a) pressure surface at 50 percent span, (b) suction surface at 50 percent span, (c) pressure surface at 90 percent span, (d) suction surface at 90 percent span.

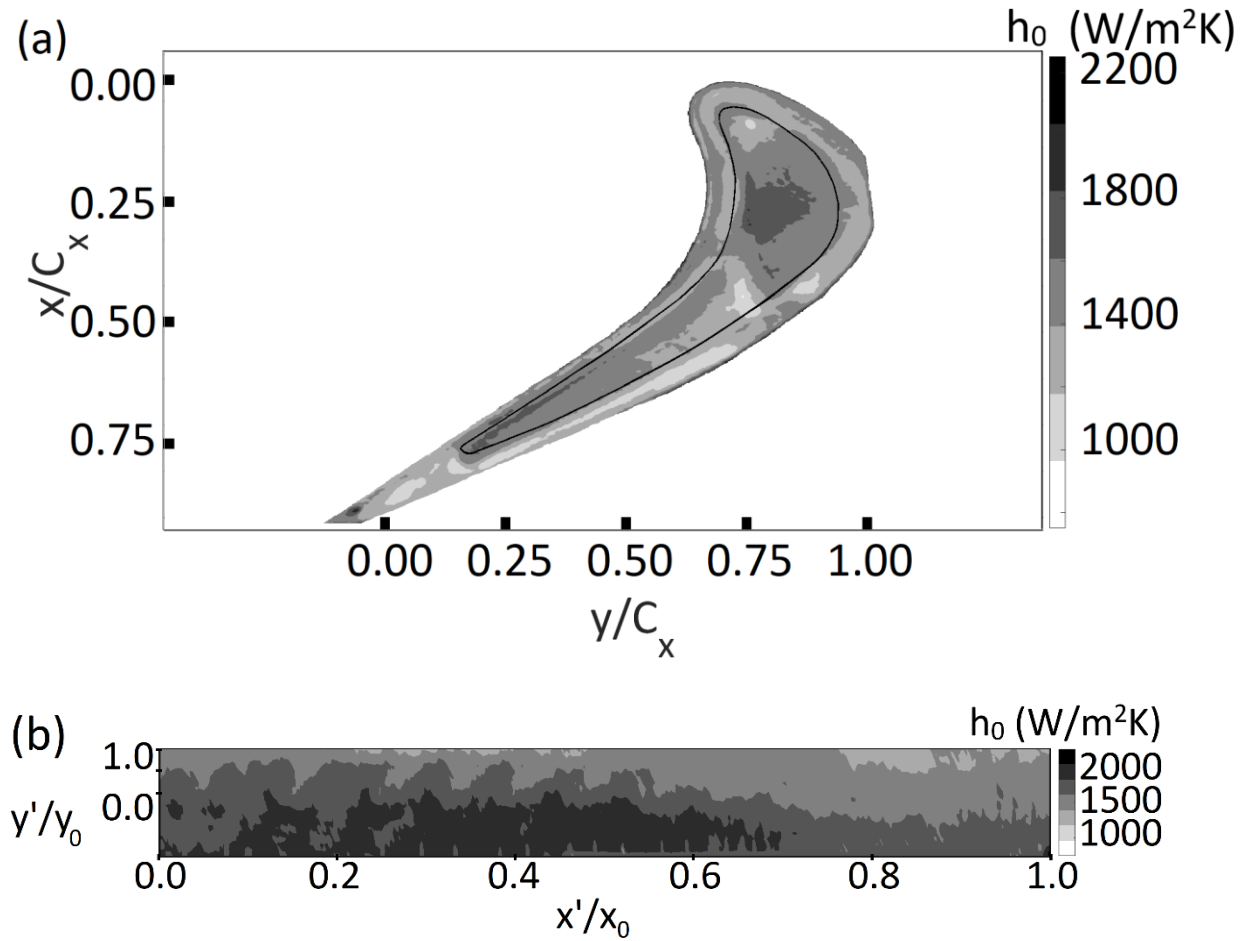


Figure 6. Heat transfer coefficient baseline with no film cooling. (a) Heat transfer coefficient along the squealer tip surface. (b) Heat transfer coefficient along the upper pressure side of the blade

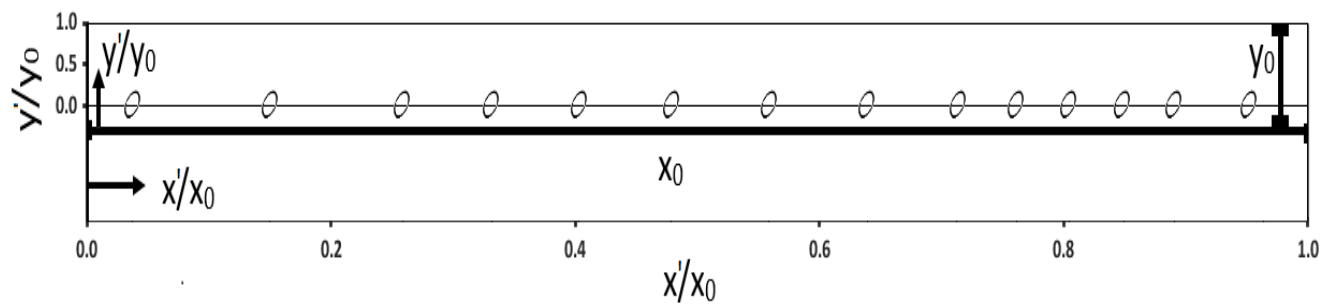
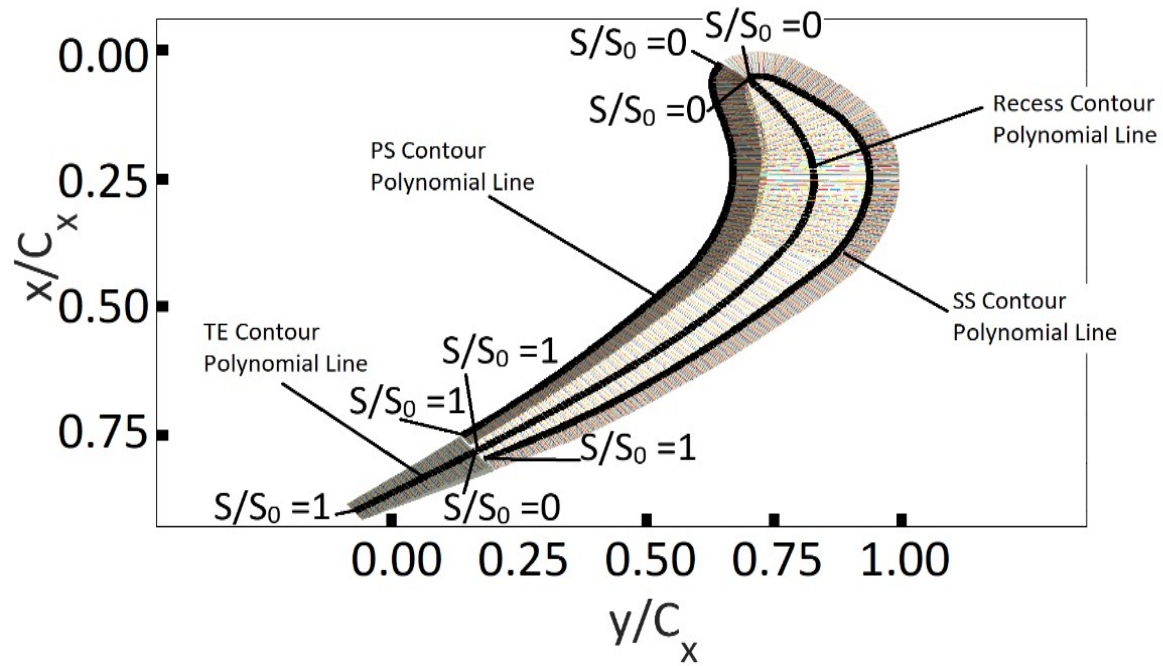


Figure 7. Heat transfer coefficient baseline with no film cooling. (a) Heat transfer coefficient along the squealer tip surface. (b) Heat transfer coefficient along the upper pressure side of the blade

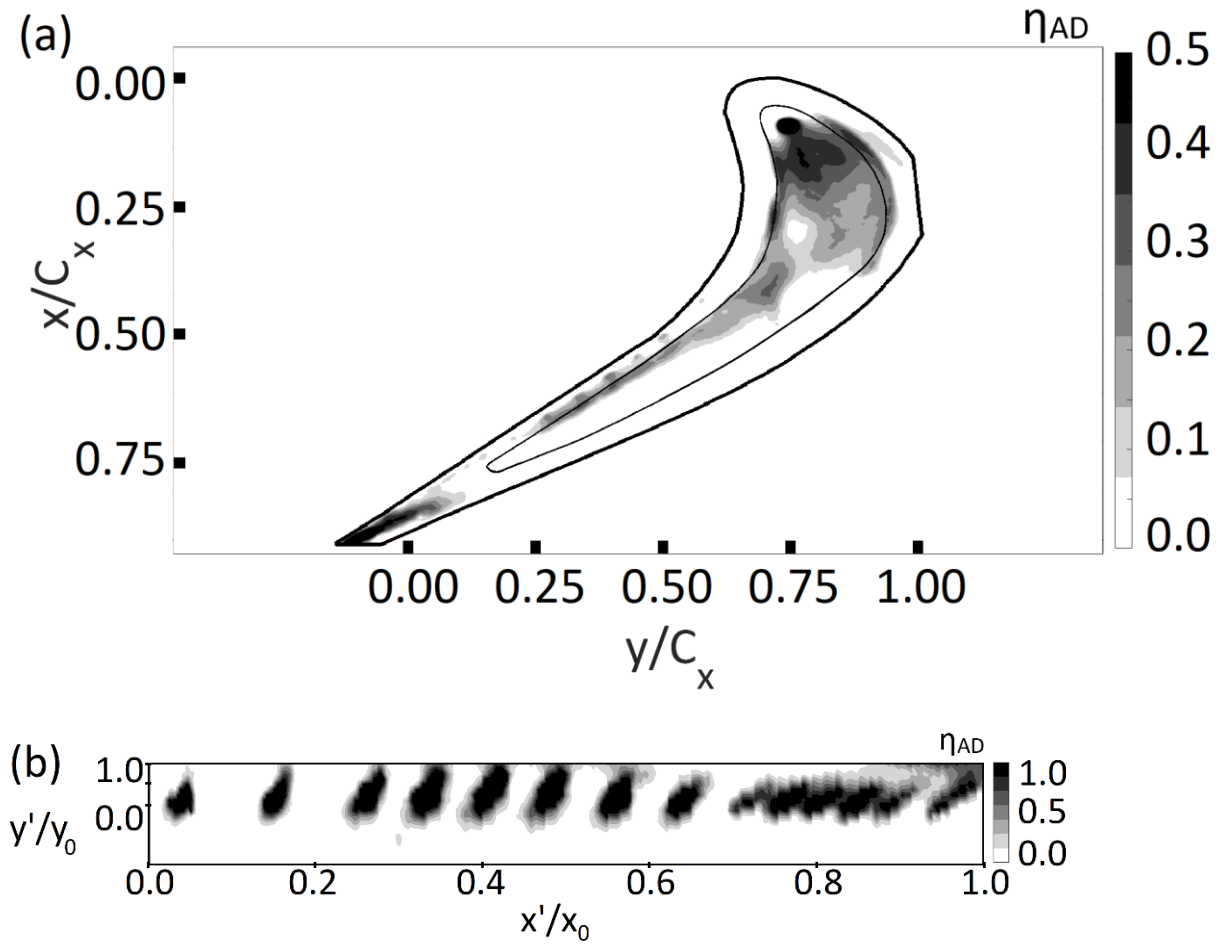


Figure 8. Adiabatic film cooling effectiveness data. (a) Along the squealer tip with $BR_u=1.89$, $BR_d=1.04$. (b) Along the upper pressure side with $BR_u=1.94$, $BR_d=0.97$.

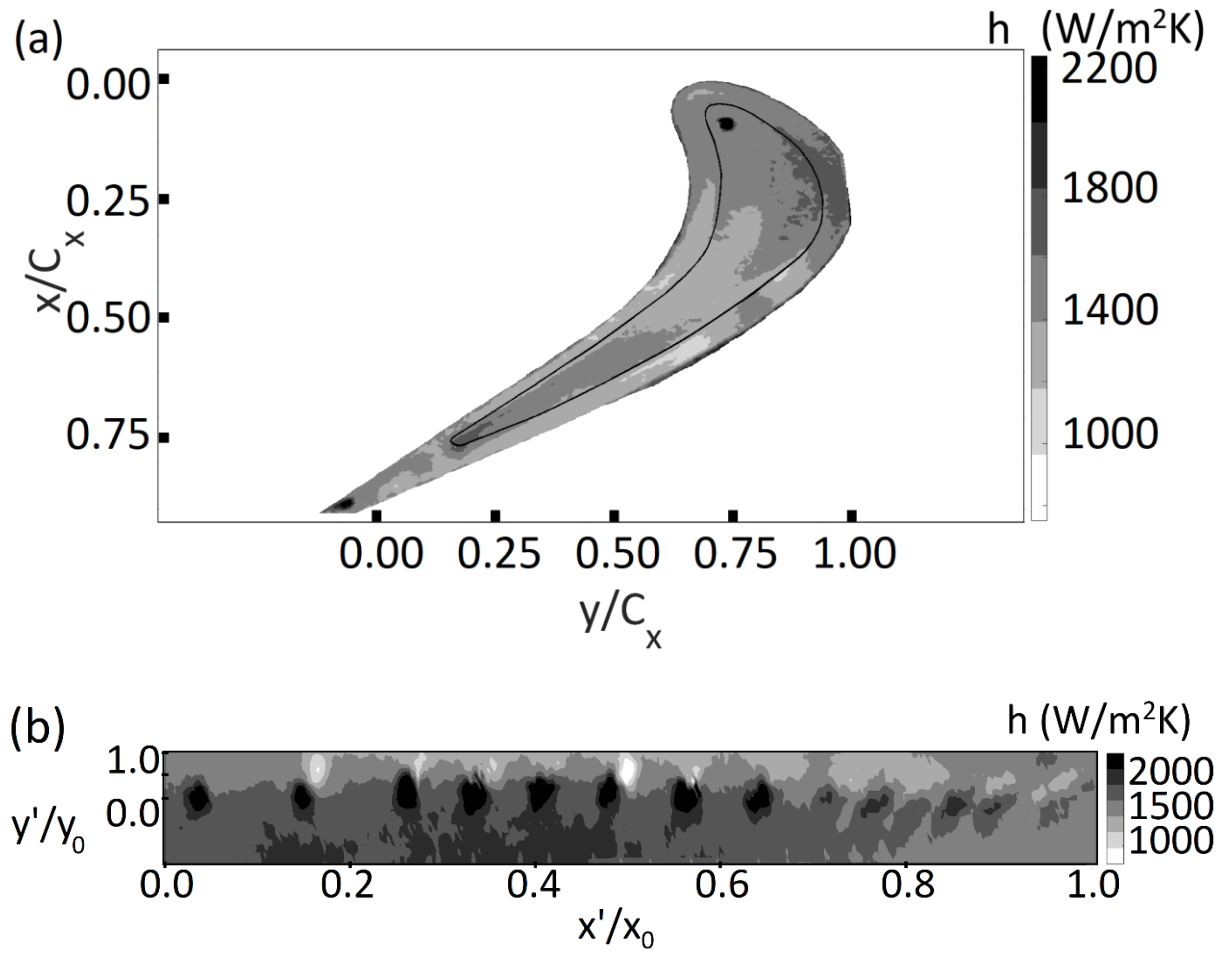


Figure 9. Heat transfer coefficient data. (a) Along the squealer tip with $BR_u=1.89$, $BR_d=1.04$.

(b) Along the upper pressure side with $BR_u=1.94$, $BR_d=0.97$.

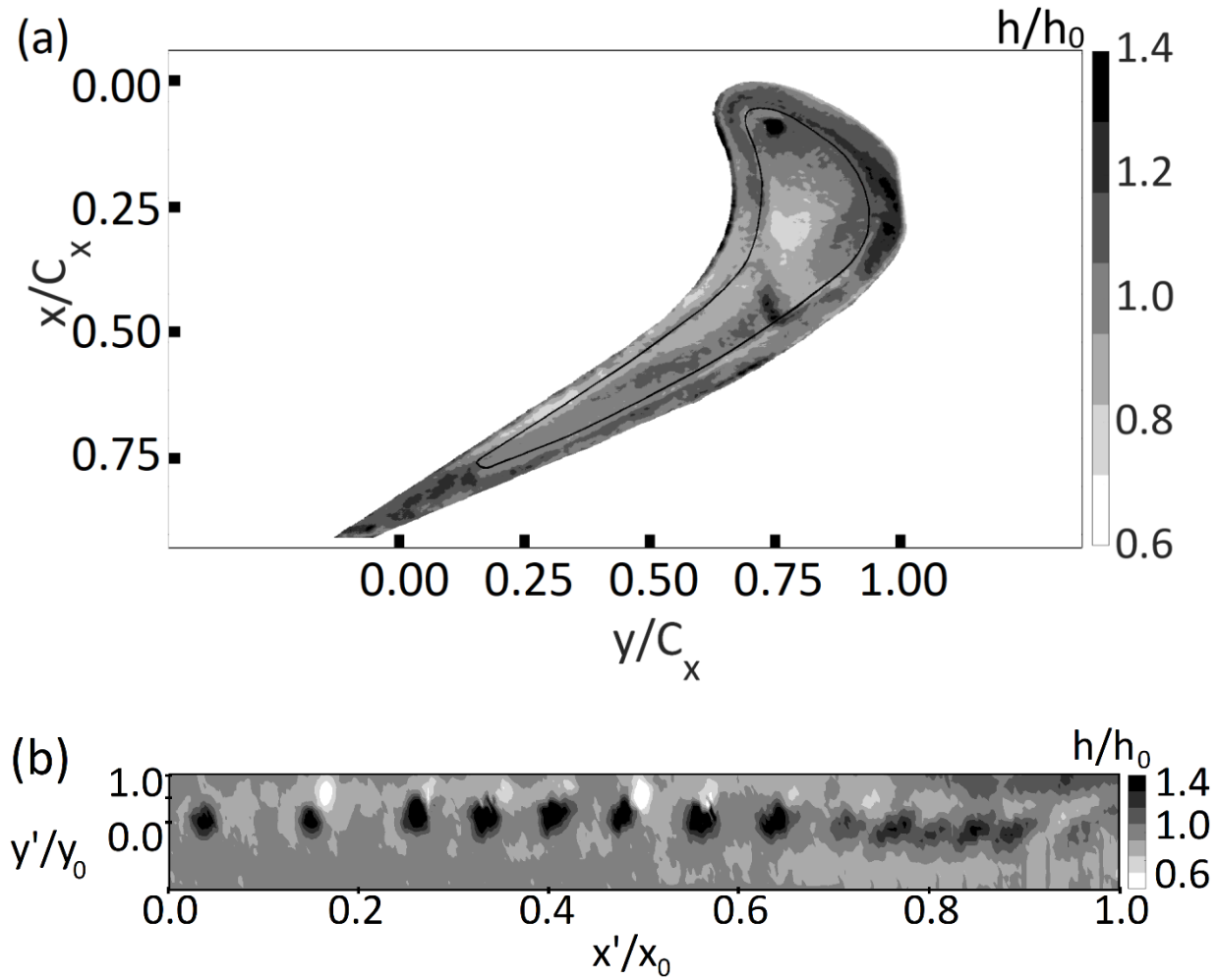


Figure 10. Heat transfer coefficient ratio data. (a) Along the squealer tip with $BR_u=1.89$, $BR_d=1.04$. (b) Along the upper pressure side with $BR_u=1.94$, $BR_d=0.97$.

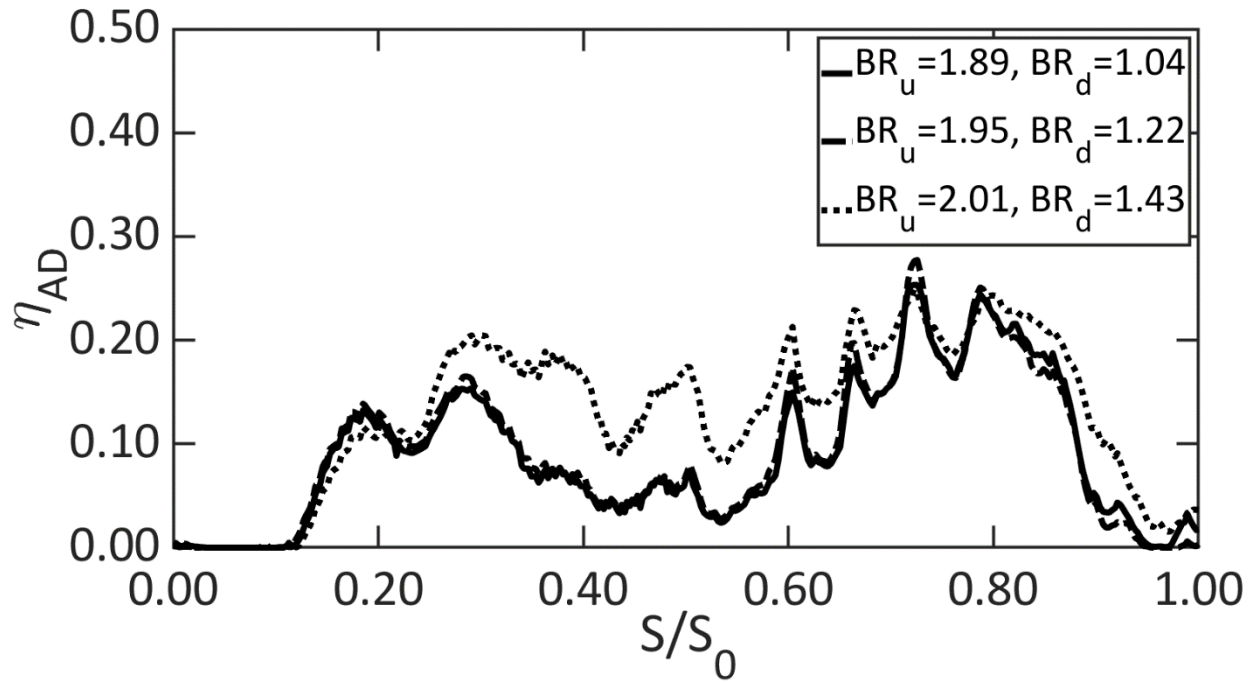


Figure 11. Line-averaged adiabatic film cooling effectiveness variation with 8D film cooling, with blowing ratios $BR_u=1.89$, $BR_d=1.04$, $BR_u=1.95$, $BR_d=1.22$ and $BR_u=2.01$, $BR_d=1.43$ with a tip gap of 1.2 mm along the pressure side rim.

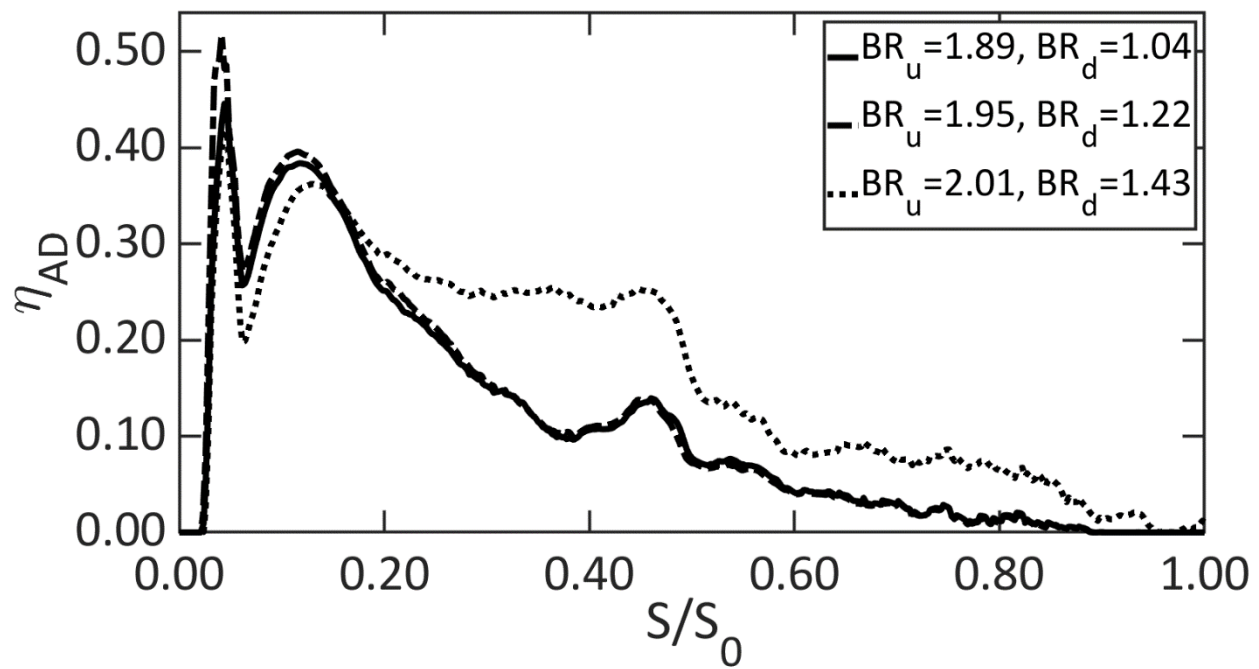


Figure 12. Line-averaged adiabatic film cooling effectiveness variation with 8D film cooling, with blowing ratios $BR_u=1.89$, $BR_d=1.04$, $BR_u=1.95$, $BR_d=1.22$ and $BR_u=2.01$, $BR_d=1.43$ with a tip gap of 1.2 mm along the squealer tip recess region.

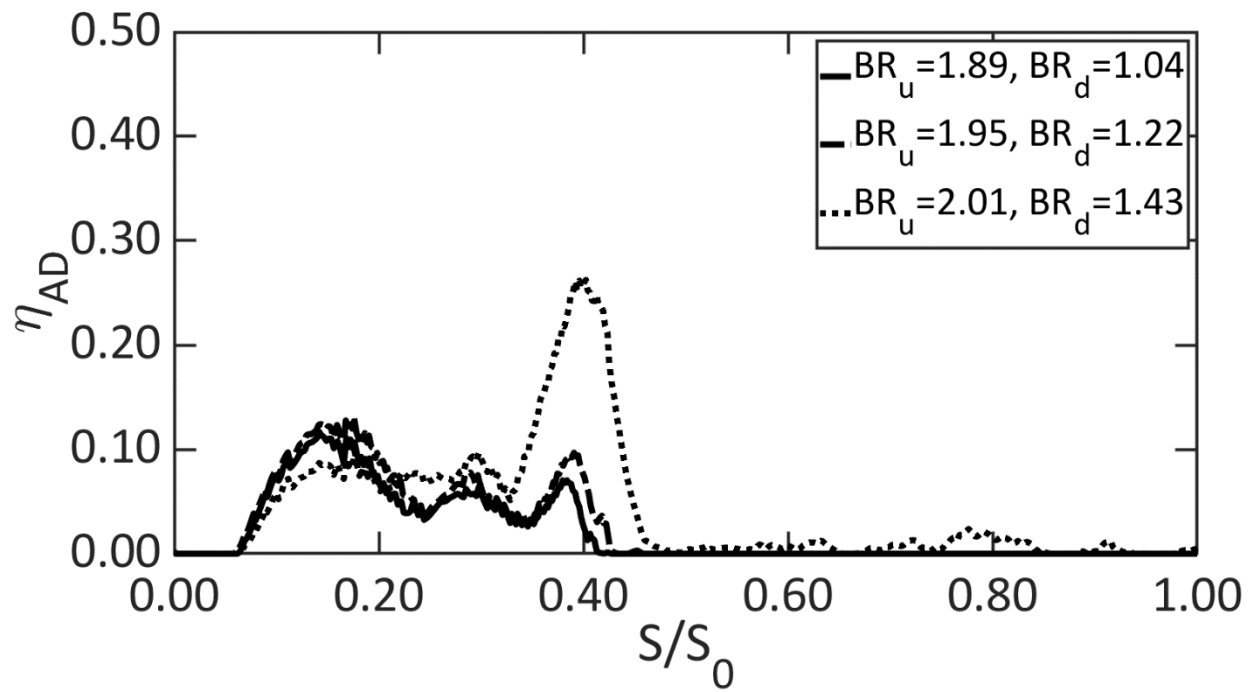


Figure 13. Line-averaged adiabatic film cooling effectiveness variation with 8D film cooling, with blowing ratios $BR_u=1.89$, $BR_d=1.04$, $BR_u=1.95$, $BR_d=1.22$ and $BR_u=2.01$, $BR_d=1.43$ with a tip gap of 1.2 mm along the suction side rim.

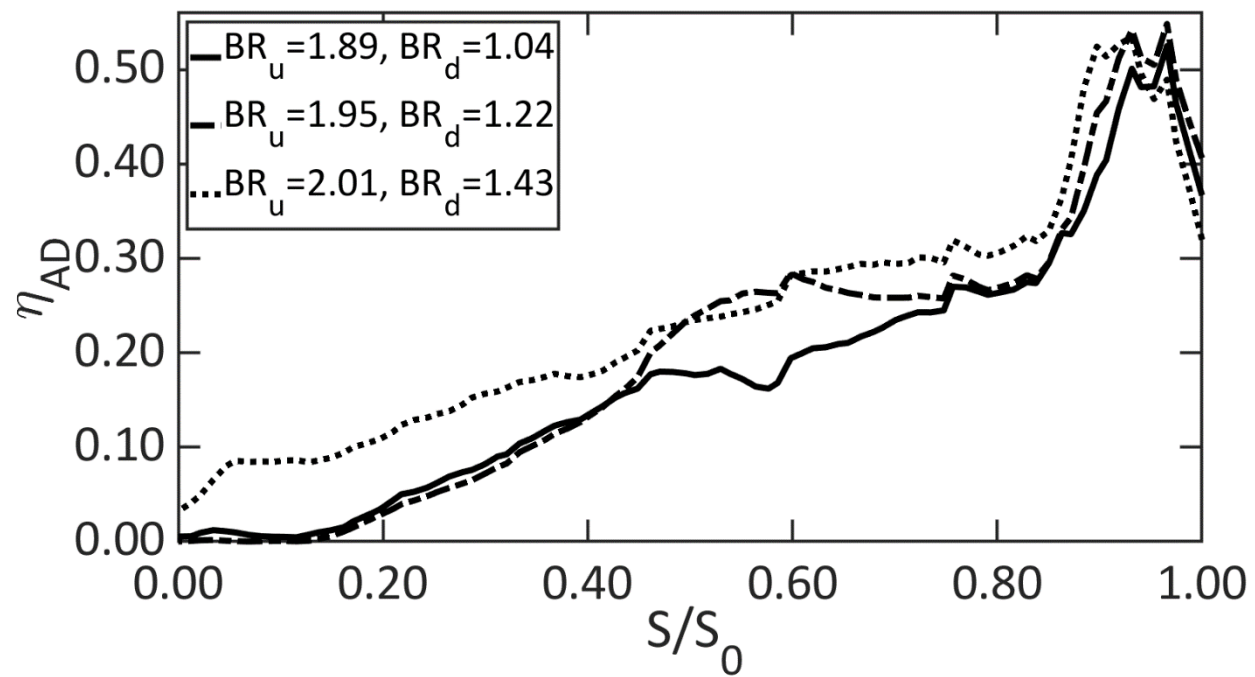


Figure 14. Line-averaged adiabatic film cooling effectiveness variation with 8D film cooling, with blowing ratios $BR_u=1.89$, $BR_d=1.04$, $BR_u=1.95$, $BR_d=1.22$ and $BR_u=2.01$, $BR_d=1.43$ with a tip gap of 1.2 mm along the trailing edge region.

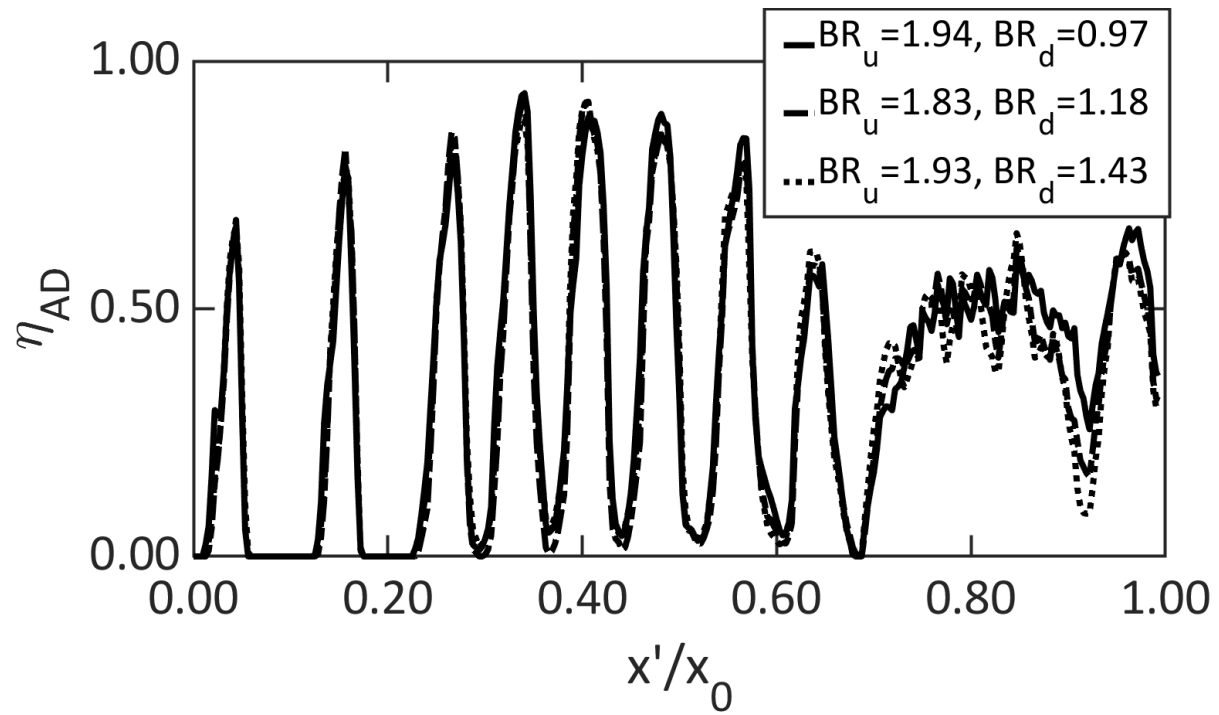


Figure 15. Variation of adiabatic film cooling effectiveness with x'/x_0 (with averaging in the y'/y_0 direction) with blowing ratio for a tip gap of 1.2 mm along the upper pressure side of the 8D blade.

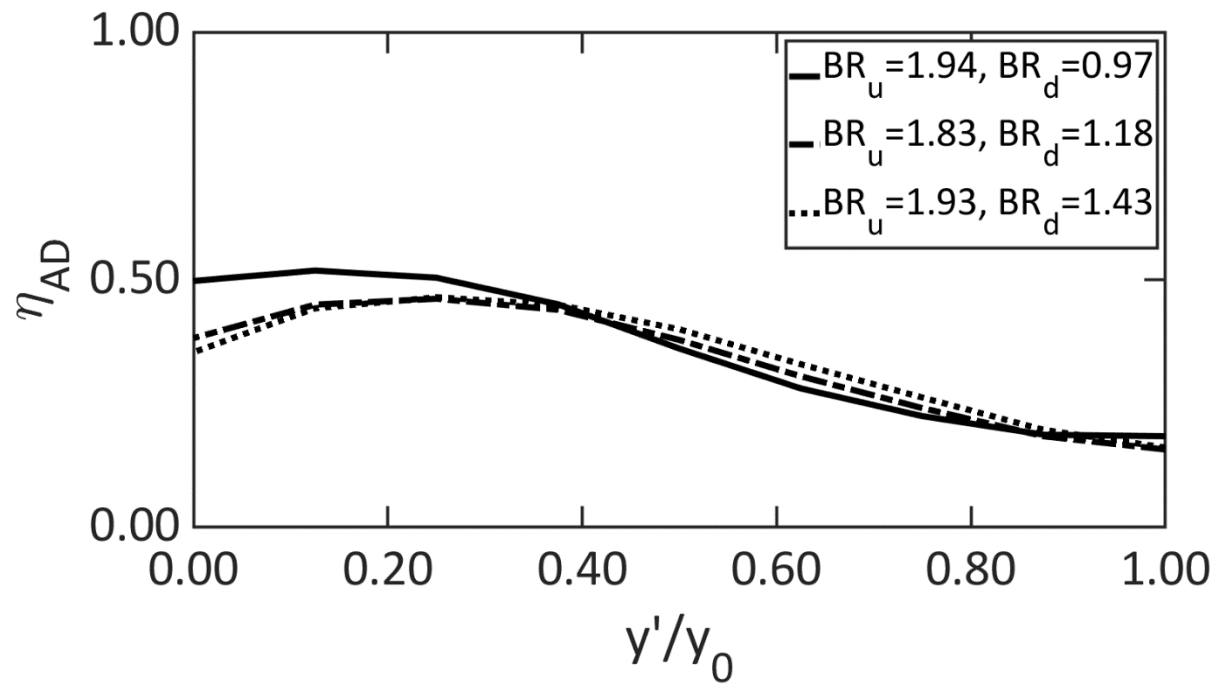


Figure 16. Variation of adiabatic film cooling effectiveness with y'/y_0 (with averaging in the x'/x_0 direction) with blowing ratio for a tip gap of 1.2 mm along the upper pressure side of the 8D blade.

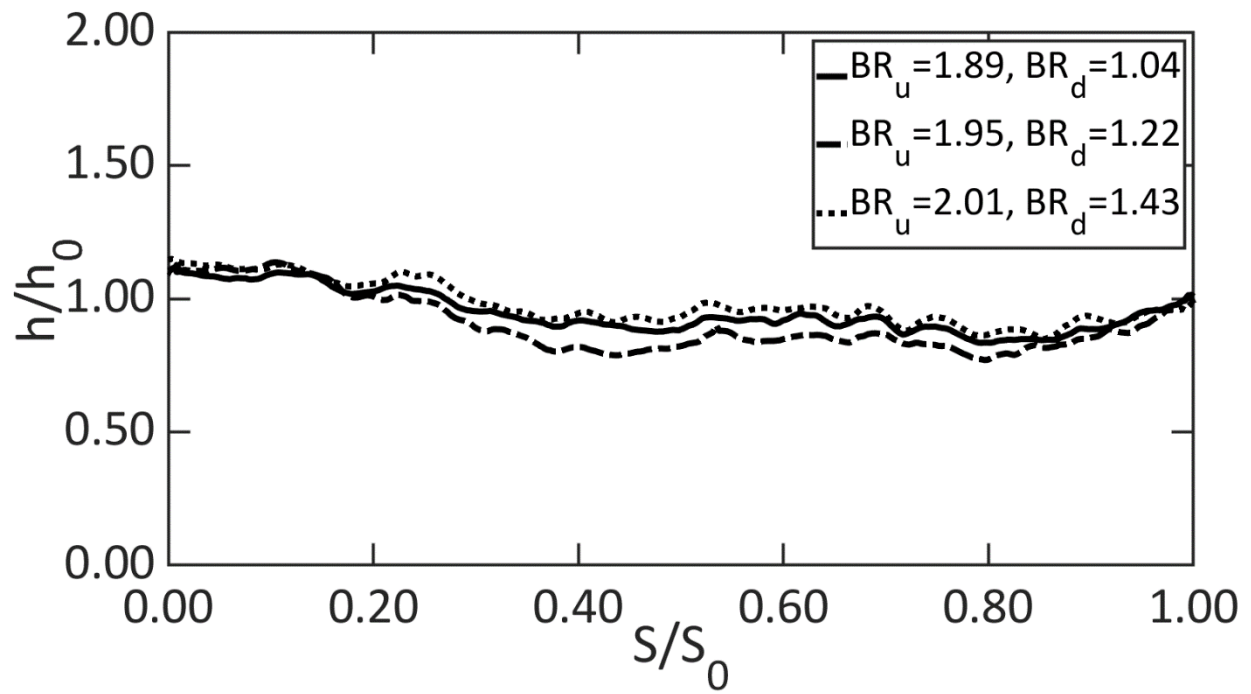


Figure 17. Line-averaged heat transfer coefficient ratio variation with 8D film cooling, with blowing ratios $BR_u=1.89$, $BR_d=1.04$, $BR_u=1.95$, $BR_d=1.22$ and $BR_u=2.01$, $BR_d=1.43$ with a tip gap of 1.2 mm along the pressure side rim.

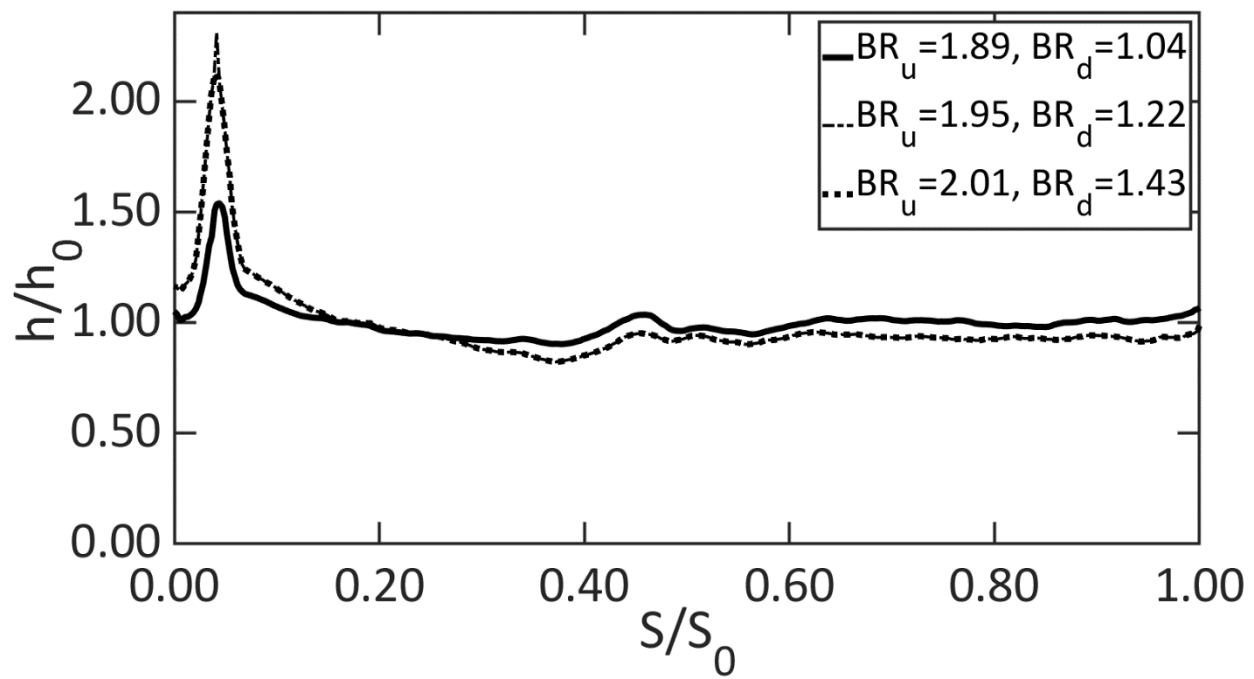


Figure 18. Line-averaged heat transfer coefficient ratio variation with 8D film cooling, with blowing ratios $BR_u=1.89$, $BR_d=1.04$, $BR_u=1.95$, $BR_d=1.22$ and $BR_u=2.01$, $BR_d=1.43$ with a tip gap of 1.2 mm along the squealer tip recess region.

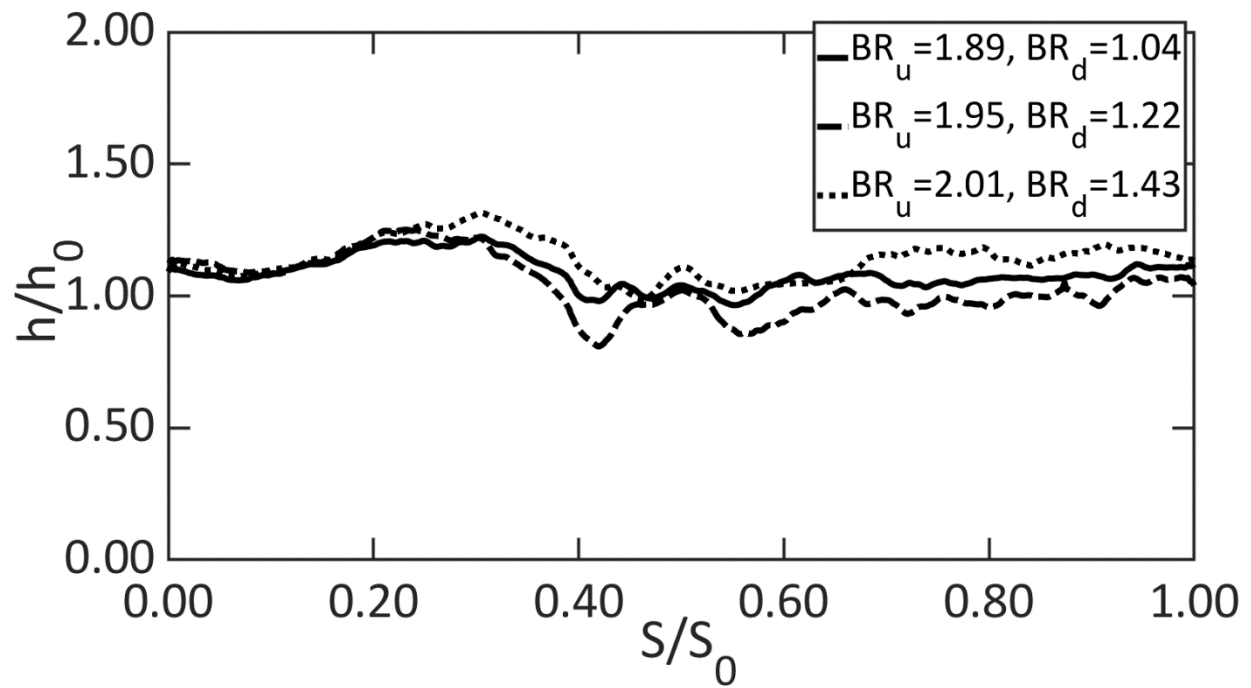


Figure 19. Line-averaged heat transfer coefficient ratio variation with 8D film cooling, with blowing ratios $BR_u=1.89, BR_d=1.04, BR_u=1.95, BR_d=1.22$ and $BR_u=2.01, BR_d=1.43$ with a tip gap of 1.2 mm along the suction side rim.

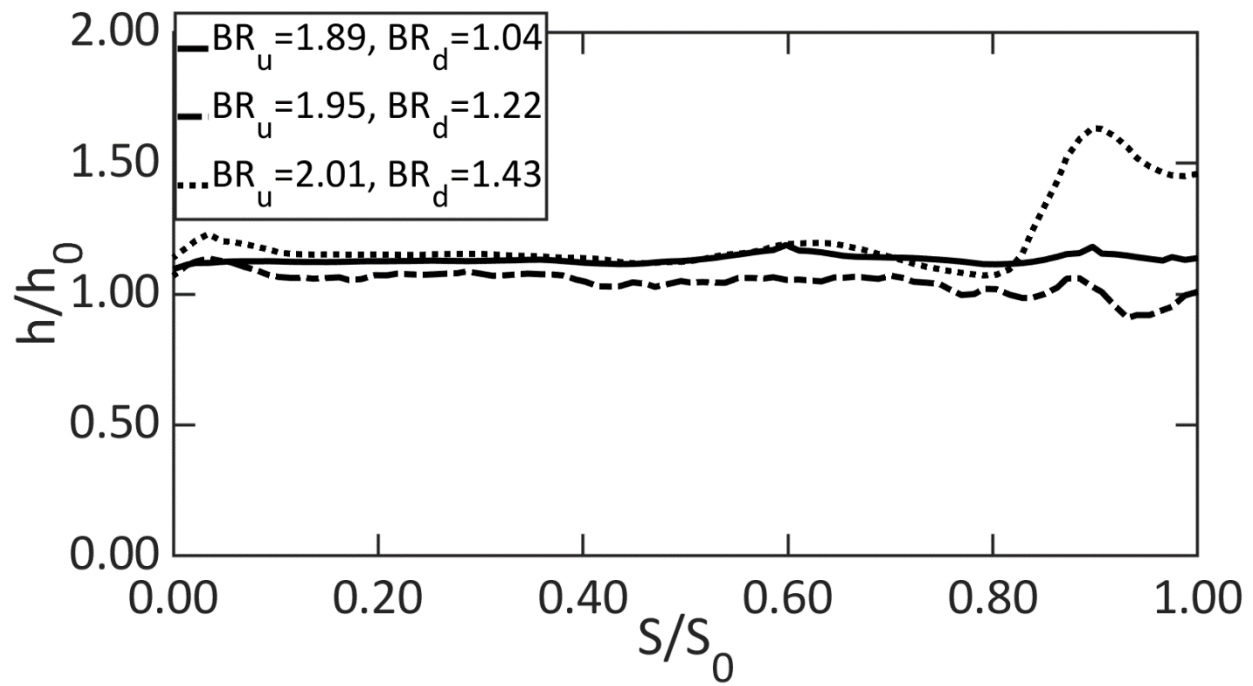


Figure 20. Line-averaged heat transfer coefficient ratio variation with 8D film cooling, with blowing ratios $BR_u=1.89$, $BR_d=1.04$, $BR_u=1.95$, $BR_d=1.22$ and $BR_u=2.01$, $BR_d=1.43$ with a tip gap of 1.2 mm along the trailing edge region.

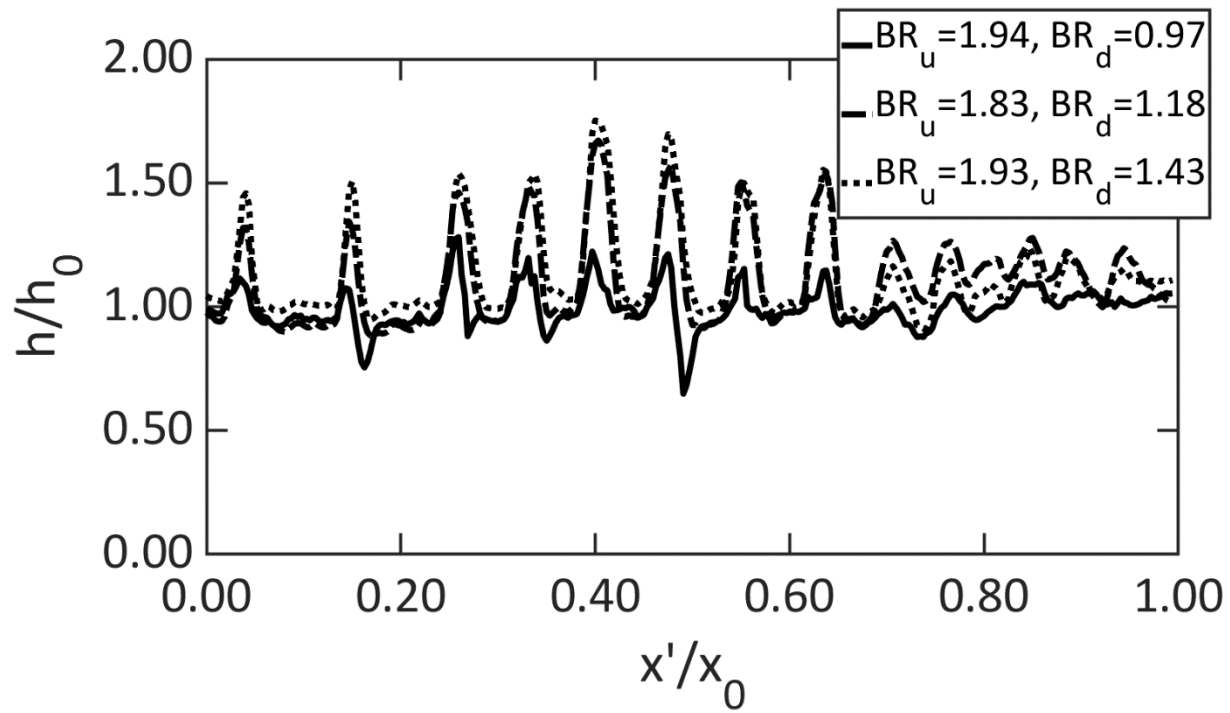


Figure 21. Variation of heat transfer coefficient ratio with x'/x_0 (with averaging in the y'/y_0 direction) with blowing ratio for a tip gap of 1.2 mm along the upper pressure side of the 8D blade.

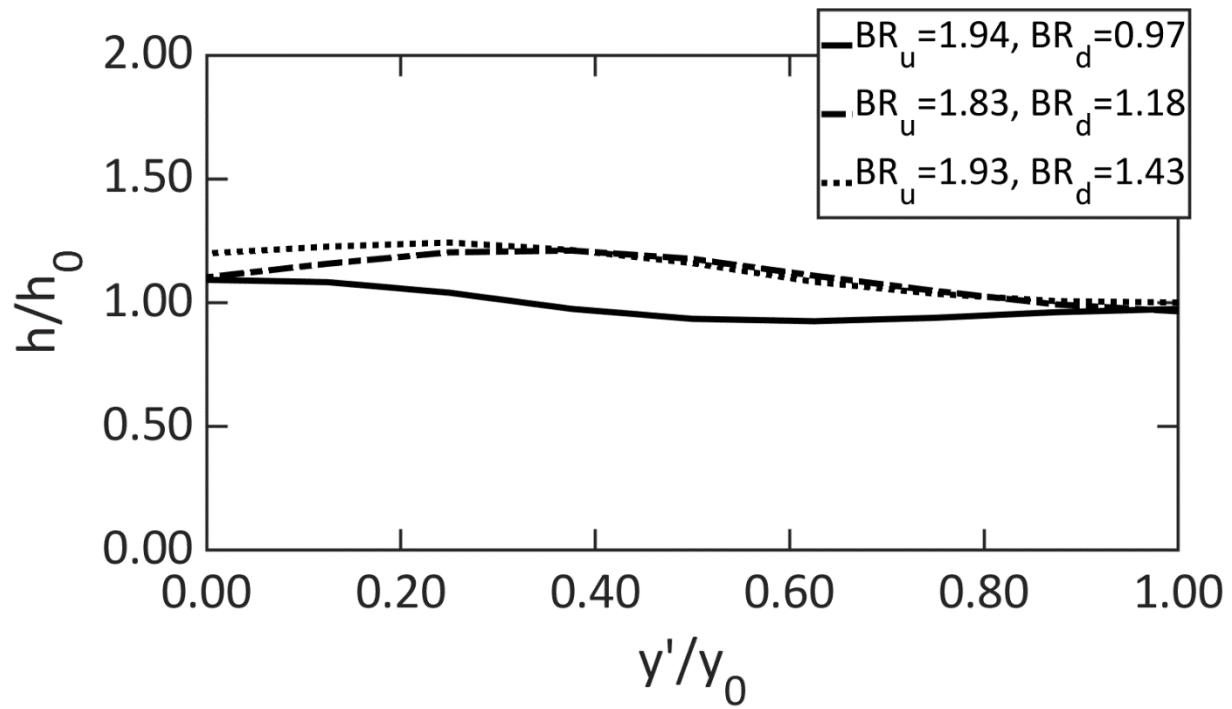


Figure 22. Variation of heat transfer coefficient ratio with y'/y_0 (with averaging in the x'/x_0 direction) with blowing ratio for a tip gap of 1.2 mm along the upper pressure side of the 8D blade.

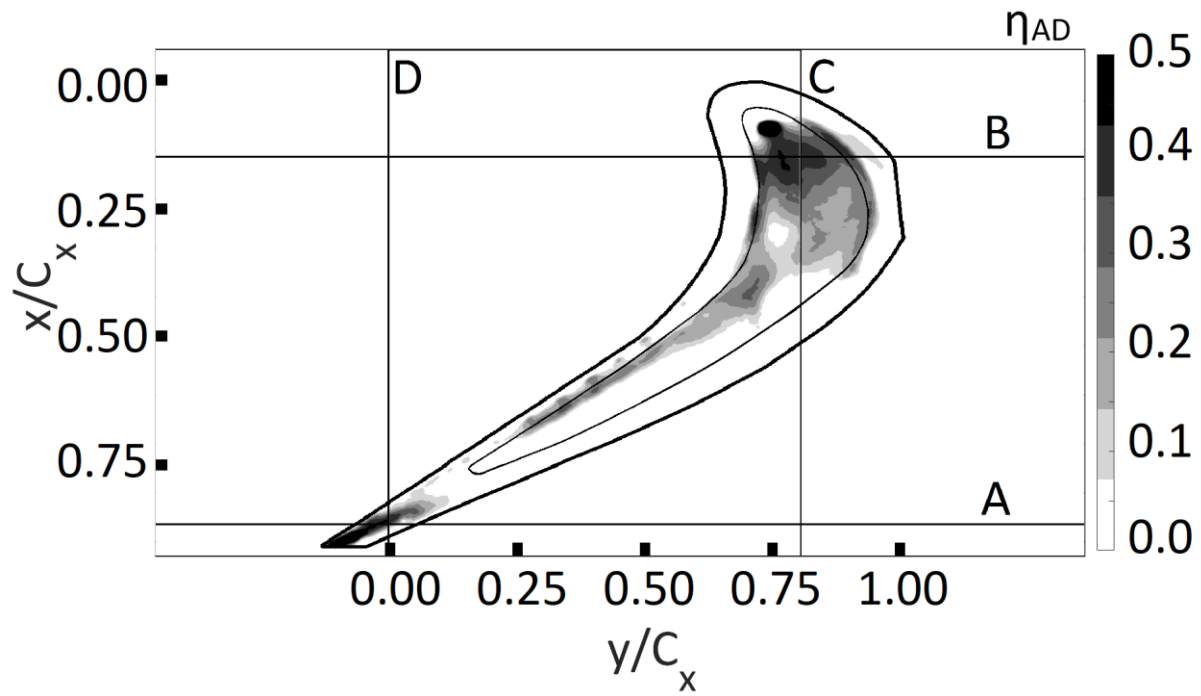


Figure 23. Line locations A, B, C, and D shown for adiabatic film cooling effectiveness data along the squealer tip surface with blowing ratios $BR_u=1.89$, $BR_d=1.04$ and a tip gap of 1.2 mm.

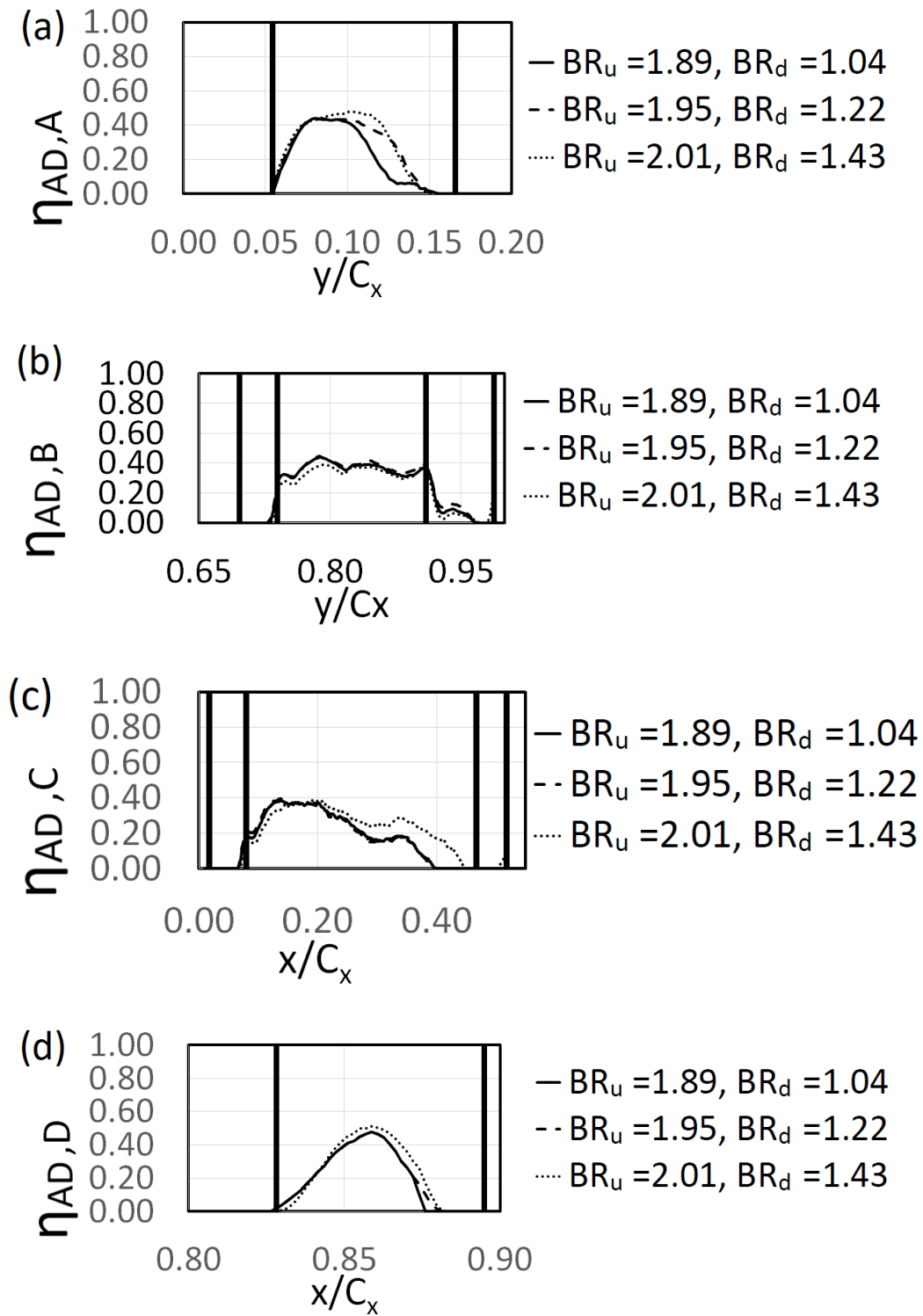


Figure 24. Variation of adiabatic film cooling effectiveness with blowing ratio (a) for line location A, (b) for line location B, (c) for line location C, (d) for line location D.

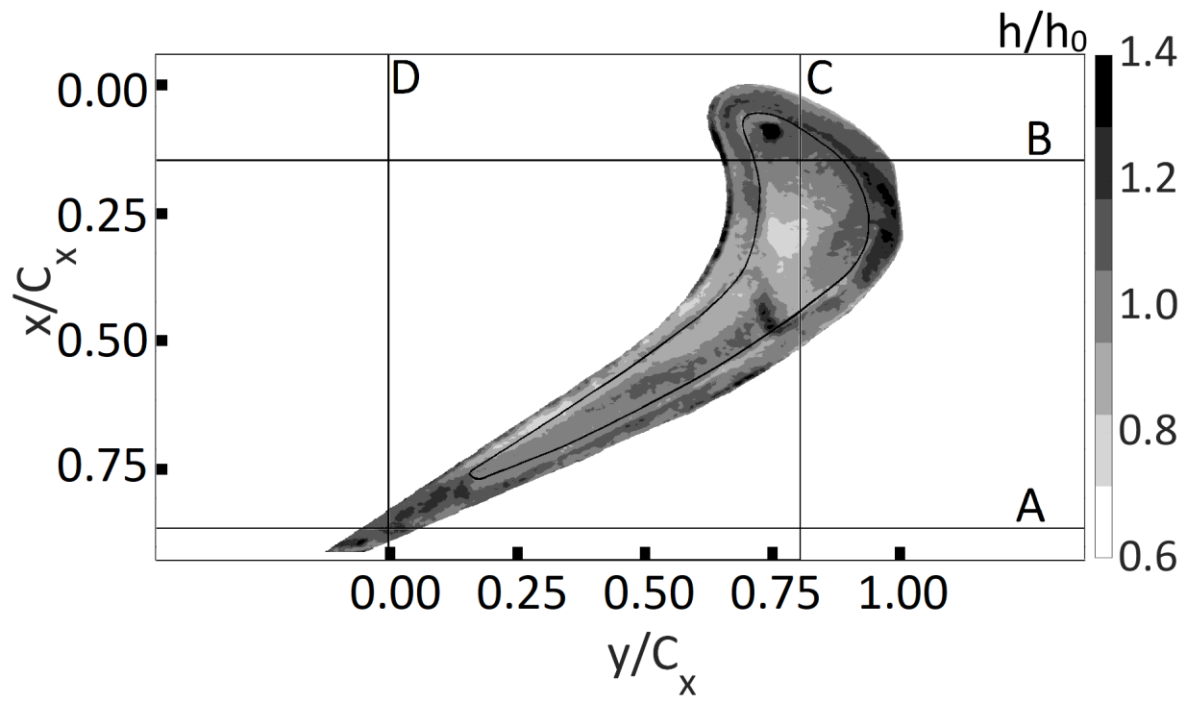


Figure 25. Line locations A, B, C, and D shown for heat transfer coefficient ratio data along the squealer tip surface with blowing ratios $BR_u=1.89$, $BR_d=1.04$ and a tip gap of 1.2 mm.

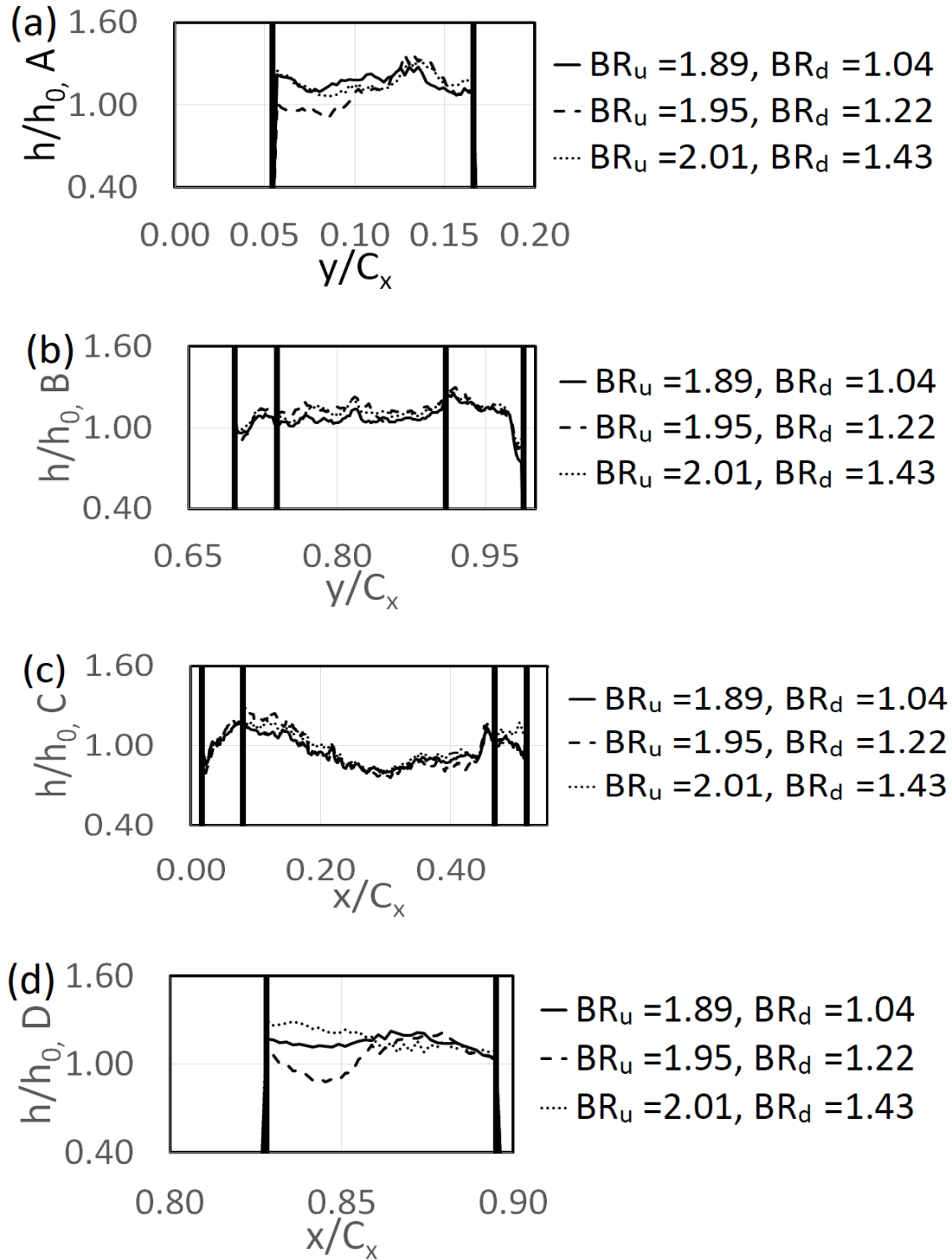


Figure 26. Variation of heat transfer coefficient ratio with blowing ratio (a) for line location A, (b) for line location B, (c) for line location C, (d) for line location D.

References

- Collopy, H., Ligrani, P.M., Xu, H., Fox, M., Effects of Tip Gap on Transonic Turbine Blade Heat Transfer Characteristics With Pressure Side Film Cooling. *International Journal of Heat and Mass Transfer*, 2022, 187: 122513
- Virdi, A.S., Zhang, Q., He, L., Li, H.D., Hunsley, R., 2013, "Aerothermal Performance of Shroudless Turbine Blade Tips with Effects of Relative Casing Motion," Paper NoTBTS2013-2021, ASME Turbine Blade Symposium.
- Wheeler, A.P.S., Atkins, N.R., He, L., 2011, "Turbine Blade Tip Heat Transfer in Low Speed and High Speed Flows," *Journal of Turbomachinery*, 133, pp. 041025.